JOURNAL OF PETROLOGY

Journal of Petrology, 2019, Vol. 60, No. 3, 619–648
doi: 10.1093/petrology/egz008
Advance Access Publication Date: 7 February 2019
Original Article

OXFORD

Composition of the Chilled Marginal Rocks of the Panzhihua Layered Intrusion, Emeishan Large Igneous Province, SW China: Implications for Parental Magma Compositions, Sulfide Saturation History and Fe–Ti Oxide Mineralization

Zhong-Jie Bai[1]*, Hong Zhong[1,2], Rui-Zhong Hu[1,2], Wei-Guang Zhu[1] and Wen-Jun Hu[1,3]

[1]State Key Laboratory of Ore Deposit Geochemistry, Institute of Geochemistry, Chinese Academy of Sciences, Guiyang 550081, China; [2]College of Earth and Planetary Sciences, University of Chinese Academy of Sciences, Beijing 100049, China; [3]Department of Earth Sciences, The University of Hong Kong, Hong Kong, China

*Corresponding author. Present address: State Key Laboratory of Ore Deposit Geochemistry, Institute of Geochemistry, Chinese Academy of Sciences, 99 West Lincheng Road, Guiyang 550081, China. Telephone: +86 851 85891820. Fax: +86 851 85891664. E-mail: baizhongjie@vip.gyig.ac.cn

Received August 12, 2018; Accepted January 29, 2019

ABSTRACT

The chilled marginal rocks of the Panzhihua layered intrusion of the Emeishan Large Igneous Province (ELIP), SW China, including microgabbros and olivine–phyric gabbros, are similar to coeval high-Ti basalts in the Panzhihua area in both major and trace element compositions. The olivine–phyric gabbros are characterized by depleted Nd isotopic compositions ($\varepsilon_{Nd}(t) = +1{\cdot}15$ to $+4{\cdot}18$) and initial $^{87}Sr/^{86}Sr$ (0·7043–0·7052) similar to those of the Panzhihua layered series and the associated high-Ti basalts. The microgabbros have similar initial $^{87}Sr/^{86}Sr$ (0·7045 to 0·7054) but more enriched Nd isotopic compositions ($\varepsilon_{Nd}(t) = -1{\cdot}49$ to $+0{\cdot}06$), suggesting that the magma was contaminated by lower crustal materials. The microgabbros have average compositions of 45·5 wt % SiO_2, 8·5 wt % MgO and 13·5 wt % FeO_T, which are within the ranges of the associated high-Ti basalts. The average TiO_2 content in the microgabbros is 2·7 wt %, which is close the lower end of the high-Ti basalts ($TiO_2 = 2{\cdot}5$ wt %). Coexisting olivine–phyric gabbros contain abundant coarse-grained olivine phenocrysts (20–60 vol. %) and fine-grained clinopyroxene + plagioclase. Cr-spinel inclusions enclosed in the olivine phenocrysts have highly variable Cr_2O_3 contents (5·9–33·8 wt %) within a single host crystal. Using the average composition of the chilled microgabbros as a starting composition, MELTS simulation indicates that such a magma can well reproduce the mineral compositions and assemblages in the overlying layered series of the Panzhihua intrusion, implying that the average composition of the chilled microgabbros is similar to the parental magma for these rocks. The chilled marginal rocks (microgabbros and olivine–phyric gabbros) have high S contents (up to 1·48 wt %), but low abundances of platinum group elements (PGE). The total amounts of PGE in these rocks vary from 8·6 to 32·9 ppb. The Cu/Pd ratios of these rocks range between $0{\cdot}75 \times 10^4$ and $3{\cdot}44 \times 10^4$, which are significantly higher than mantle values and indicate previous sulfide removal from the magma at depth. The parental magma with elevated Cu/Pd contains more MgO (>8 wt %) than the coeval PGE-undepleted basalts (MgO = 3·2–4·5 wt %), indicating that sulfide saturation was not triggered by extensive fractionation. Nevertheless, the mantle-like Sr–Nd–O–S isotopic compositions of the mineralized Fe–Ti oxide-bearing intrusions of the ELIP

also suggest that S saturation was not related to crustal contamination. We suggest that the contamination and fractionation of an early pulse of mantle-derived S-undersaturated magma in a deep-seated magma chamber most likely caused S saturation and sulfide liquid segregation within the lower crust. The chilled microgabbro formed by influx of the residual PGE-depleted, but Nd isotope enriched, magma. A subsequent pulse of S-undersaturated magma then reached S saturation during the early stages of differentiation as a result of the resorption of the previously formed sulfide liquid. This Nd isotope and PGE-depleted magma was then successively emplaced into a shallow crustal chamber along with captured olivine, generating the olivine–phyric gabbros and associated Fe–Ti oxide deposits. Our results support the interpretation that the Fe–Ti oxides directly crystallized from a basaltic parental magma at an early stage of differentiation and then formed the ore layers by gravitational settling. The composition of the parental magma does not support the hypothesis that the early crystallization of Fe–Ti oxides was controlled by high Fe and Ti concentrations in the parental magma. The moderately high oxygen fugacity (FMQ + 1∼FMQ + 2·5) of the parental magma, which was inherited from an oxidized mantle source, may account for the early saturation of Fe–Ti oxides.

Key words: chilled margin; parental magma composition; olivine slurry; Fe–Ti oxide deposit; sulfide saturation; Emeishan LIP

INTRODUCTION

Mafic–ultramafic layered intrusions provide geological evidence of the processes of differentiation and evolution of basaltic magmas within crustal magma chambers, as well as commonly hosting major economic Fe–Ti–V–Cr and Ni–Cu–platinum group element (PGE) ore deposits. Nevertheless, the genesis of the mineral deposits that are hosted by these layered intrusions remains controversial. This means that determining the compositions of the parental magmas that formed these layered intrusions and the geochemical evolution of these magmas is an important step in understanding the ore-forming processes recorded within the intrusions.

Although previous studies have examined the Panzhihua magmatic Fe–Ti–(V) deposit, the origin of this mineralization remains debated and a number of models have been proposed to explain the origin of the Fe–Ti oxides. Zhou *et al.* (2005) and Xing *et al.* (2014) suggested that the oxide ores formed from immiscible Fe–Ti-rich oxide melts within a magma chamber, whereas Zhou *et al.* (2013) proposed that the mantle-derived Fe–Ti-rich mafic magmas that formed the deposit experienced two stages of immiscible liquid separation during the formation of the Fe–Ti oxide mineralization. Other studies have suggested that the oxide mineralization within the intrusion formed as a result of the accumulation of Fe–Ti oxides that crystallized from an Fe–Ti-rich basaltic magma within a magma chamber (e.g. Ganino *et al.*, 2008; Pang *et al.*, 2008*a*, 2008*b*, 2009; Song *et al.*, 2013; Bai *et al.*, 2014). However, Howarth *et al.* (2013) argued that the main Fe–Ti oxide ore layers within the Panzhihua intrusion did not form *in situ*, but instead were derived from crystal-rich Ti-magnetite slurries that were generated in a deeper magma chamber.

Numerous layered intrusions host magnetite-bearing cumulus rocks that are enriched in sulfides and PGE, including the Rio Jacaré intrusion in Brazil (Sa *et al.*, 2005) and the Stella intrusion in South Africa (Maier *et al.*, 2003). However, all of the Fe–Ti oxide mineralized intrusions within the ELIP (including the Panzhihua, Hongge, Baima and Taihe intrusions) have low concentrations of PGE, with the exception of the Xinjie intrusion (Bai *et al.*, 2012*a*; Howarth & Prevec, 2013; Zhang *et al.*, 2013; Shellnutt *et al.*, 2015; She *et al.*, 2017). In addition, the evolution of, and controls on, the sulfide saturation status of these Fe–Ti oxide mineralized intrusions remain unclear, but might explain the lack of giant Cu–Ni–(PGE) sulfide deposits within the ELIP.

Determining how Fe–Ti oxide ore deposits form and the sulfide saturation status of a magmatic system require an estimation of the composition of the parental magma. However, the parental magma composition of the Panzhihua deposit remains controversial. The main approaches employed to constrain the parental magma composition of the Panzhihua intrusion include: (1) bulk mass summation (Zhou *et al.*, 2005); (2) estimation using selected gabbro samples (Zhang *et al.*, 2009); (3) estimation using ultramafic dikes (Hou *et al.*, 2012); and (4) estimation using coeval Emeishan flood basalts and associated melt inclusions (Ganino *et al.*, 2008; Pang *et al.*, 2008*a*; Song *et al.*, 2013). These various studies have yielded different parental magma compositions as a result of their dependency on different assumptions, meaning that the resulting compositions are highly variable, especially in terms of FeO, TiO_2 and MgO contents. Consequently, it is difficult to determine the exact compositions of the parental magmas of the Panzhihua intrusion.

Fine-grained rocks within the marginal zones of mafic–ultramafic intrusions have long been thought to be potentially representative of parental magma compositions (Wager, 1960). The best example of this is the

Bushveld Complex, where different sections of Marginal Zone rocks (e.g. the B-1, B-2 and B-3 rocks) are thought to represent parental magma compositions for different zones within the complex (Cawthorn *et al.*, 1981; Sharpe, 1981; Cawthorn & Davies, 1983; Sharpe & Hulbert, 1985; Barnes *et al.*, 2010; Wilson, 2012, 2015; Maier *et al.*, 2016).

This study presents new compositional data from the marginal zone of the Panzhihua intrusion and uses these data to estimate the composition of the parental magma for the intrusion and to determine the processes that drove these magmas to sulfide saturation and formed the Fe–Ti oxide deposit that is hosted by the intrusion.

GEOLOGICAL SETTING

Emeishan Large Igneous Province

The ~260 Ma ELIP (Fig. 1) consists of a volcanic sequence and spatially and temporally associated intrusive rocks that were erupted or emplaced over a short period of time (Chung & Jahn, 1995; Xu *et al.*, 2001; Zhou *et al.*, 2002; Xiao *et al.*, 2004; Zhong *et al.*, 2011*a*; Shellnutt *et al.*, 2012). The ELIP crops out over an area of 5×10^5 km^2 in southwestern China and northern Vietnam. The ELIP volcanic sequence is dominated by flood basalts and subordinate amounts of picrites, pyroclastic rocks and rhyolitic and trachytic flows. The volcanic sequence varies in thickness from 5 km in the western part of the ELIP to several hundred metres in the eastern part (Chung & Jahn, 1995). The Emeishan basalts have been divided into high-Ti ($TiO_2 > 2{\cdot}5$ wt %, $Ti/Y > 500$) and low-Ti ($TiO_2 < 2{\cdot}5$ wt %, $Ti/Y < 500$) series (Xu *et al.*, 2001; Xiao *et al.*, 2004). The high-Ti (HT) series has been further divided into three sub-types based on chemical composition: HT1 lavas contain higher TiO_2 (4·25 wt %) and $Fe_2O_3^T$ (15·71 wt %) than HT2 lavas ($TiO_2 = 2{\cdot}86$ wt %, $Fe_2O_3^T = 14{\cdot}12$ wt %), whereas HT3 basalts are more primitive than both the HT1 and HT2 lavas (Xu *et al.*, 2001). The majority of the flood basalts within the inner zone of the ELIP have been eroded away as a result of uplift, with the remnant flood basalts generally cropping out within the intermediate zone of the LIP (Xu & He, 2007; Fig. 1). In comparison, the intrusive rocks of the ELIP are generally exposed within the Panzhihua–Xichang area (Fig. 1). These intrusive units are dominated by mafic–ultramafic intrusions, granites and syenites. Felsic plutons within the Emeishan LIP are commonly spatially and temporally associated, and are co-genetic with mafic–ultramafic intrusions (Shellnutt & Zhou, 2007; Xu *et al.*, 2007; Zhong *et al.*, 2007). Sporadically distributed basalts within the Pan–Xi area include the Ertan HT2 basalts (Xu *et al.*, 2001) that crop out close to the Panzhihua intrusion and the Longzhoushan HT1 basalts (Qi *et al.*, 2008) that crop out close to the Hongge and Xinjie intrusions (Fig. 1).

Mafic–ultramafic intrusions and associated Fe–Ti–(V) deposits

Several mafic–ultramafic intrusions within the ELIP contain giant magmatic Fe–Ti–(V) oxide deposits or Ni–Cu–(PGE) sulfide mineralization. Small sill or dike-like mafic–ultramafic intrusions (e.g. Limahe (Tao *et al.*, 2008); Jinbaoshan (Tao *et al.*, 2007); Zhubu (Tang *et al.*, 2013); Baimazhai (Wang & Zhou, 2006); Yangliuping (Song *et al.*, 2003)) host magmatic Cu–Ni–(PGE)-bearing sulfide mineralization that is located within both inner and outer zones. These mineralized intrusions generally contain peridotite, websterite, olivine pyroxenite, pyroxenite and gabbro units, and some of the mineralization is Ni–Cu-rich. Consequently, this mineralization is divided into Ni–Cu deposits (e.g. Limahe and Baimazhai) and Ni–Cu–PGE deposits (e.g. Yangliuping) based on PGE content (Song *et al.*, 2008). In addition, other deposits (e.g. Jinbaoshan) are Ni–Cu-poor (i.e. sulfide-poor) but are PGE-rich and are hence classified as PGE deposits (Wang *et al.*, 2005). The relatively large layered intrusions that host the giant magmatic Fe–Ti oxide deposits are generally located within the inner zone (Pan–Xi area) of the ELIP. These include the Panzhihua (Zhou *et al.*, 2005; Pang *et al.*, 2008*b*), Hongge (Bai *et al.*, 2012*b*), Baima (Zhang *et al.*, 2012; Liu *et al.*, 2014*a*, 2014*b*), Taihe (She *et al.*, 2014; Bai *et al.*, 2016), Wuben (Bai *et al.*, 2019) and Xinjie (Zhong *et al.*, 2004) giant deposits and dozens of other medium to small tonnage deposits. These intrusions contain total ore reserves of ~7209 Mt Fe_2O_3, ~559 Mt TiO_2 and ~17·4 Mt V_2O_3 at average grades of 27 wt % FeO, 10·6 wt % TiO_2 and 0·24 wt % V_2O_3 (Ma *et al.*, 2003; Zhong *et al.*, 2005). The Fe–Ti oxide ore layers are generally located at the base of these intrusions, or within their lower parts. The Hongge and Xinjie intrusions comprise (from base to top) olivine clinopyroxenite, clinopyroxenite and gabbro units, whereas the Panzhihua, Baima, Wuben and Taihe intrusions are dominated by gabbro. The large Panzhihua, Hongge, Baima and Taihe Fe–Ti mineralized intrusions do not contain Cu–Ni–(PGE) sulfide mineralization, although the Xinjie intrusion contains some sulfide mineralization (Bai *et al.*, 2012*a*; Howarth & Prevec, 2013; Zhang *et al.*, 2013; Shellnutt *et al.*, 2015; She *et al.*, 2017). Of note, the Xinjie intrusion is much smaller than the other large Fe–Ti oxide mineralized layered intrusions within the ELIP.

PANZHIHUA INTRUSION

The NE–SW-striking Panzhihua layered intrusion hosts the second largest magmatic Fe–Ti oxide deposit in China. The deposit contains 1333 Mt of ore reserves at an average grade of ~43 wt % FeO, ~12 wt % TiO_2 and ~0·3 wt % V_2O_5 (Ma *et al.*, 2003). It is a sill-like body that dips 50°–60° NW and is located to the west of the regional Panzhihua Fault. The gabbroic intrusion was directly emplaced into late Neoproterozoic dolomitic limestones of the Dengying Formation and is in thrust

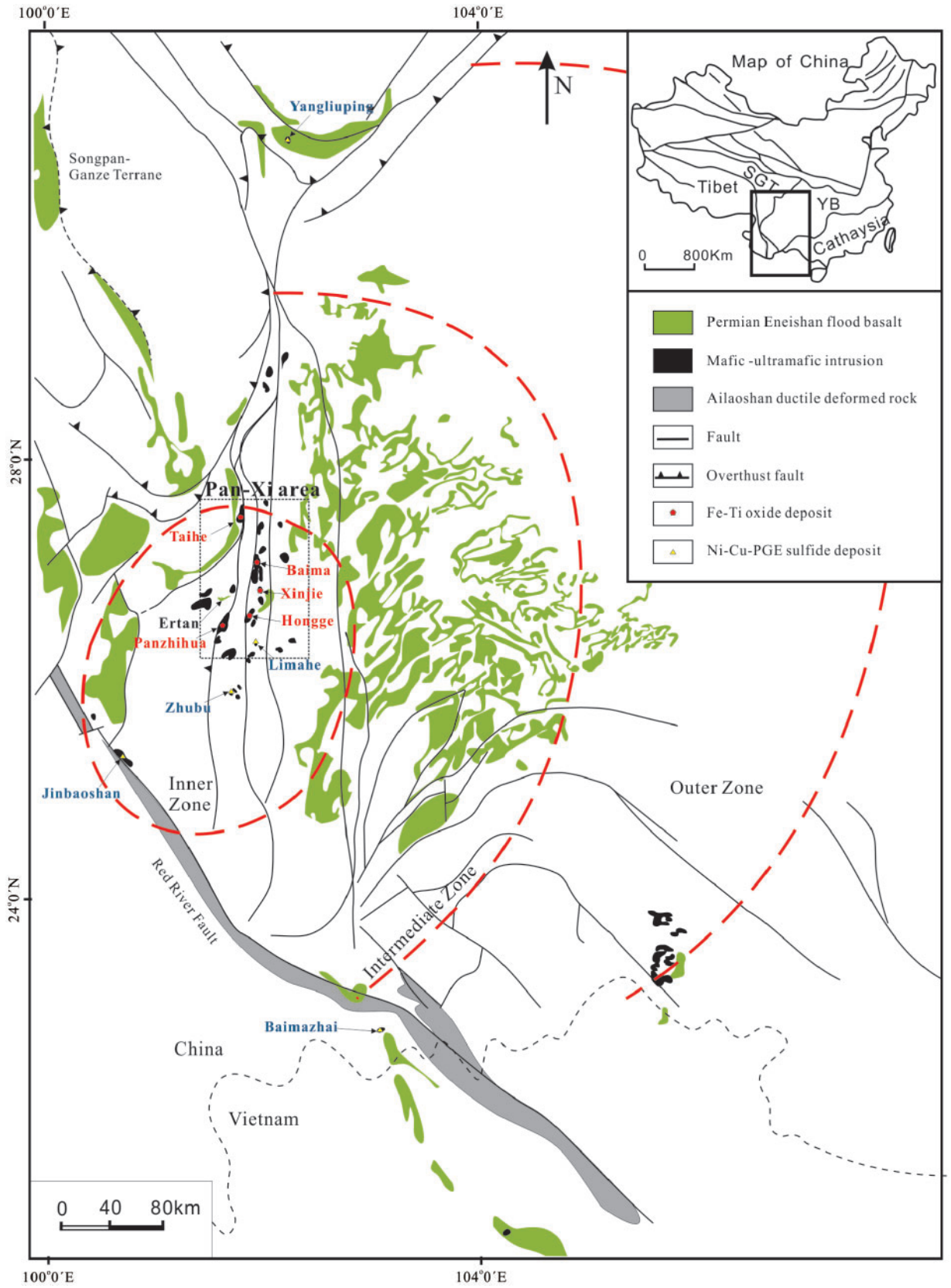

Fig. 1. Distribution of continental flood basalts and contemporaneous mafic–ultramafic layered intrusions hosting Fe–Ti oxide deposits and mafic–ultramafic sills hosting Ni–Cu–(PGE) sulfide deposits in the Emeishan Large Igneous Province, South China (modified from Zhou *et al.*, 2002).

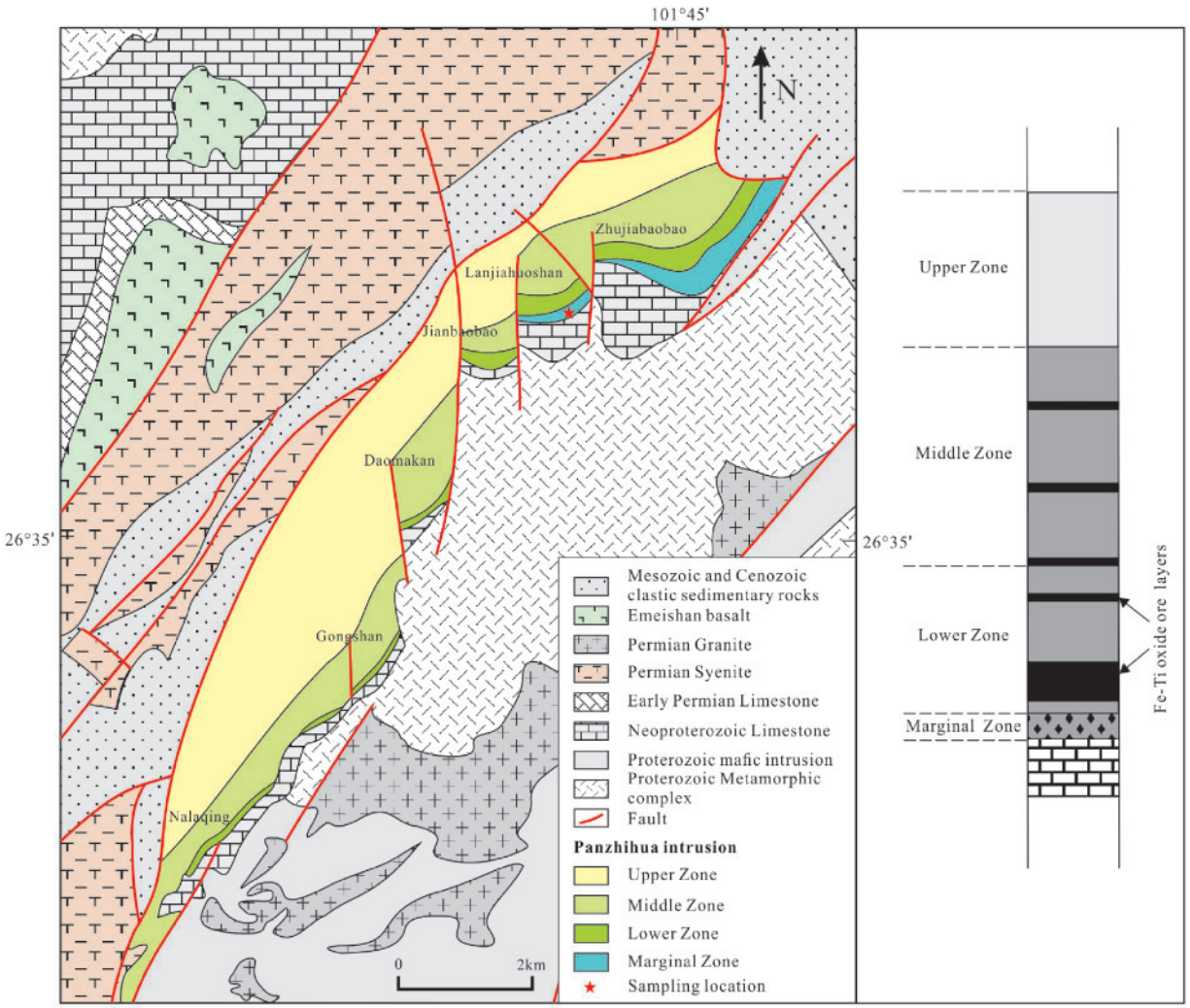

Fig. 2. Simplified geological map of the Panzhihua layered intrusion and idealized stratigraphic section (modified from Zhou *et al.*, 2005), showing sample locations.

contact with hanging wall syenite and terrestrial clastic sedimentary units. The intrusion has a maximum exposed thickness of ~2 km and crops out over an area of ~30 km^2. It is divided into the Zhujiabaobao, Lanjiahuoshan, Jianshan, Daomakan, Gongshan, Nongnongping and Nalaqing segments by a series of N–S-trending strike-slip faults (Fig. 2). The intrusion is also divided from base to top into the Marginal Zone (MGZ), Lower Zone (LZ), Middle Zone (MZ) and Upper Zone (UZ; Zhou *et al.*, 2005; Pang *et al.*, 2008*b*) based on internal structures and the extent of oxide mineralization rather than the appearance or disappearance of cumulus minerals. The highly heterogeneous Marginal Zone ranges from 0 to 40 m in thickness and consists of fine-grained and olivine–phyric gabbros that occur between the surrounding country rocks and the coarse-grained layered rocks of the intrusion. The Lower Zone is 0–110 m thick and consists of coarse-grained gabbro, melagabbro and massive oxide layers. The MGZ and LZ of the Jianshan section are compressed into a single heterogeneous zone of mixed characteristics (MGZ/LZ) (Howarth & Prevec, 2013). The massive Fe–Ti oxide ore layers are up to 60 m thick and are generally restricted to the lower part of this zone. The Middle Zone is up to 800 m thick and consists of layered gabbros that contain several layers of oxide ore. The Middle Zone has been further divided into Middle Zone a (MZa) and Middle Zone b (MZb) based on the appearance of apatite (Pang *et al.*, 2008*b*). The Upper Zone, which is 500 to 1500 m thick, is dominated by unmineralized leucogabbro assemblages and contains no apatite. The oxide assemblages in the Marginal Zone, Lower Zone and the lower part of MZa are dominated by titanomagnetite with comparatively little ilmenite. In contrast, both titanomagnetite and ilmenite are present within the upper parts of MZa and MZb at a ratio of 3:1. Rhythmic layering, marked by proportional variations in Fe–Ti oxides and silicate minerals, is developed from the base of the Lower Zone to the top of the Upper Zone, but is absent within the marginal zone of the intrusion. Pang *et al.* (2008*a*) showed the following crystallization sequence in the Panzhihua intrusion: clinopyroxene + plagioclase

+ titanomagnetite ± olivine (LZ and lower part of MZa) → olivine + clinopyroxene + plagioclase + titanomagnetite + ilmenite (upper part of MZa) →olivine + clinopyroxene+ plagioclase + titanomagnetite + ilmenite +apatite (MZb).

The marginal zone is the basal zone of the intrusion and contact with the carbonate footwall rocks. This zone is generally composed of microgabbros and olivine–phyric gabbros and has been interpreted as the chilled base of the intrusion (Pang *et al.*, 2008*a*). Most of the Lower Zone and marginal zones have been mined during half a century (Fig. 3a). Only a small amount of the chilled margins remains adjacent to the wall rocks and thus it is hard to know how they extend along the strike. However, the marginal zone occurring in different sections of the intrusion has been identified in previous studies. Zhou *et al.* (2005) and Hou *et al.* (2013) reported a marginal zone composed of fine-grained gabbro and olivine gabbro, which occurs at the base of Lanjiahuoshan section. Pang *et al.* (2009) and Howarth & Prevec (2013) also reported a marginal zone with similar rock types at the Jianshan section. This reveals that a uniform marginal zone is present at the base of the intrusion. In general, hornblende microgabbro is located at the base of the marginal zone and in direct contact with the carbonate footwall rocks. The hornblende proportion decreases away from the footwall and grades into microgabbro (Pang *et al.*, 2009). Olivine–phyric gabbro is more abundant at the upper part of the marginal zone (Howarth & Prevec, 2013). In addition, picritic dykes penetrated through the microgabbros into the dolomite wall rocks (Hou *et al.*, 2013). These dykes become gradually narrower and disappear from the marginal zone to the wall rocks. Hou *et al.* (2013) suggested that the picritic dykes and Panzhihua intrusion are co-magmatic and generated from the same staging magma chamber. Ultramafic to mafic sills that penetrated into the country rock also occur in the marginal zone of the Bushveld Complex (e.g. Cawthorn *et al.* 1981; Sharpe, 1981; Sharpe & Hulbert, 1985; Barnes *et al.* 2010). These sills together with the marginal rocks were widely used to represent the parental magma compositions of the Bushveld Complex in these studies.

The microgabbros are generally fine-grained and equigranular with grain sizes from ~50 to 300 μm (Fig. 3b). They contain intergrown subhedral clinopyroxene and plagioclase (80–90 vol. %) plus minor hornblende and Fe–Ti oxides. The proportion of hornblende gradationally increases toward the footwall contact and grades into hornblende microgabbros (Pang *et al.*, 2009). The olivine–phyric gabbros contain coarse-grained olivine hosted by a finer-grained microgabbroic matrix that consists of intergrown clinopyroxene, plagioclase and hornblende, suggesting these units represent a mixture of coarse-grained olivine and the marginal microgabbros (Fig. 3c, d). The matrix mineralogy, texture and grain size of the olivine–phyric gabbros are remarkably similar to those of the marginal microgabbros. The rounded olivine phenocrysts within these units range in abundance from 20 to 60 vol. %, range in size from 1 to 5 mm and contain tiny inclusions of Cr-spinel (Figs 3e and 4). Minor disseminated sulfides occur as part of intercumulus assemblages in the matrix and rounded inclusions within the olivine phenocrysts (Fig. 3d). The grain size is gradationally coarser at the top of the marginal zone (Howarth & Prevec, 2013).

SAMPLING AND ANALYTICAL METHODS

Twenty Marginal Zone samples for this study were collected from the Lanjiahuoshan open pit of the Panzhihua intrusion. The location of marginal zone in the Lanjiahuoshan section and the sampling location are shown in Figs 2 and 3a. Sampling intervals vary from ~1 to 2 m along the traverse (Fig. 3a). About 100 g of each sample was coarse-crushed and subsequently pulverized to <200 mesh in an agate mortar for bulk-rock geochemical analyses. The chemical compositions of olivine and Cr-spinel were determined by wavelength-dispersive X–ray analysis employing a JXA-8230 electron microprobe at the State Key Laboratory of Ore Deposit Geochemistry, Institute of Geochemistry, Chinese Academy of Sciences. These analyses for major elements used a 25 nA beam current, a 15 kV acceleration voltage, 1 μm beam size and peak counting time of 10 s. Ni and Mn in olivine were analysed using a peak counting time of 60 s. Both natural (e.g. olivine, chromite) and synthetic (metal vanadium) standards were used for calibration and the analytical precision for major and minor elements is ~2% RSD.

Whole-rock major element compositions were determined using X-ray fluorescence spectrometry at the ALS Laboratory Group, Guangzhou, China, yielding analytical precision better than 5%. S contents were determined using a C–S infrared elemental analyser, also at the ALS Laboratory Group, Guangzhou. Whole-rock trace element compositions were determined by quadrupole–inductively coupled plasma–mass spectrometry (Q–ICP–MS) employing a Perkin-Elmer Sciex ELAN DRC–e instrument housed at the State Key Laboratory of Ore Deposit Geochemistry (SKLODG), Institute of Geochemistry, Chinese Academy of Sciences, Beijing, China. Prior to analysis, powdered samples (50 mg) were dissolved in high-pressure Teflon bombs using an HF + HNO_3 mixture for 48 h at ~190°C. Signal drift during analysis was monitored using Rh and a BCR-2 standard was used to monitor analytical accuracy. The analytical precisions of the resulting trace element concentrations are generally better than 10% in relative standard deviation terms. Platinum-group elements were measured by isotope dilution (ID)–ICP–MS using an improved digestion technique (Qi *et al.*, 2011), again at SKLODG. The concentrations of the mono-isotopic element Rh were determined by external calibration using a ^{194}Pt spike as an internal standard

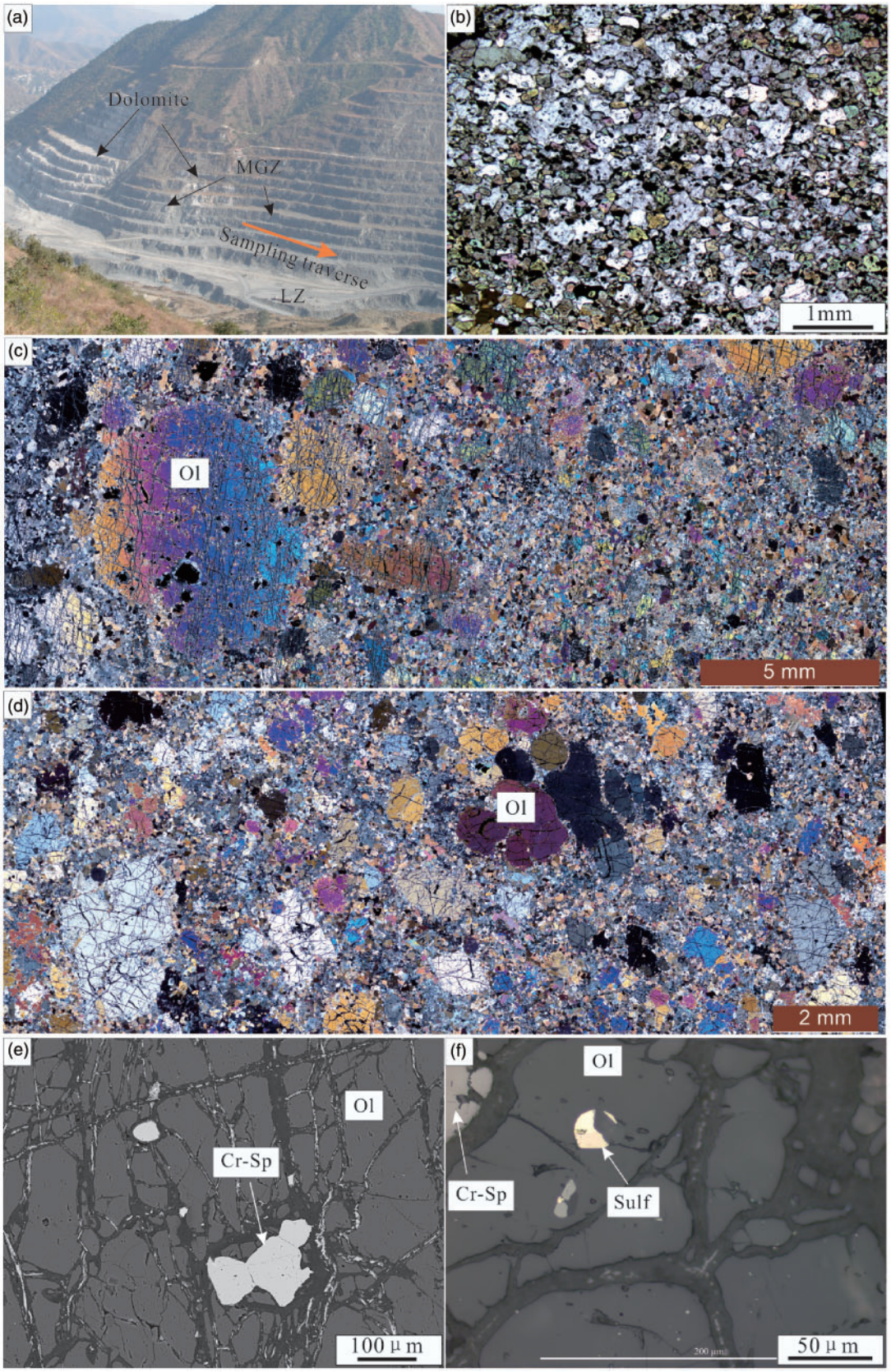

Fig. 3. (a) Overview of the Lanjiahuoshan section of the Panzhihua intrusion and (b–f) photomicrographs of representative rock textures from the marginal zone. (a) Photograph showing the location of the Marginal Zone of the Lanjiahuoshan section and the sampling location. (b) Microgabbro with a fine-grained and equigranular texture. (c, d) Olivine–phyric gabbros with coarse grained olivine set in a matrix of finer grained microgabbro. (e) BSE image showing tiny Cr-spinel inclusions hosted in rounded olivine phenocrysts. (f) BSE image showing Cr-Spinel and sulfide globules hosted in olivine phenocrysts.

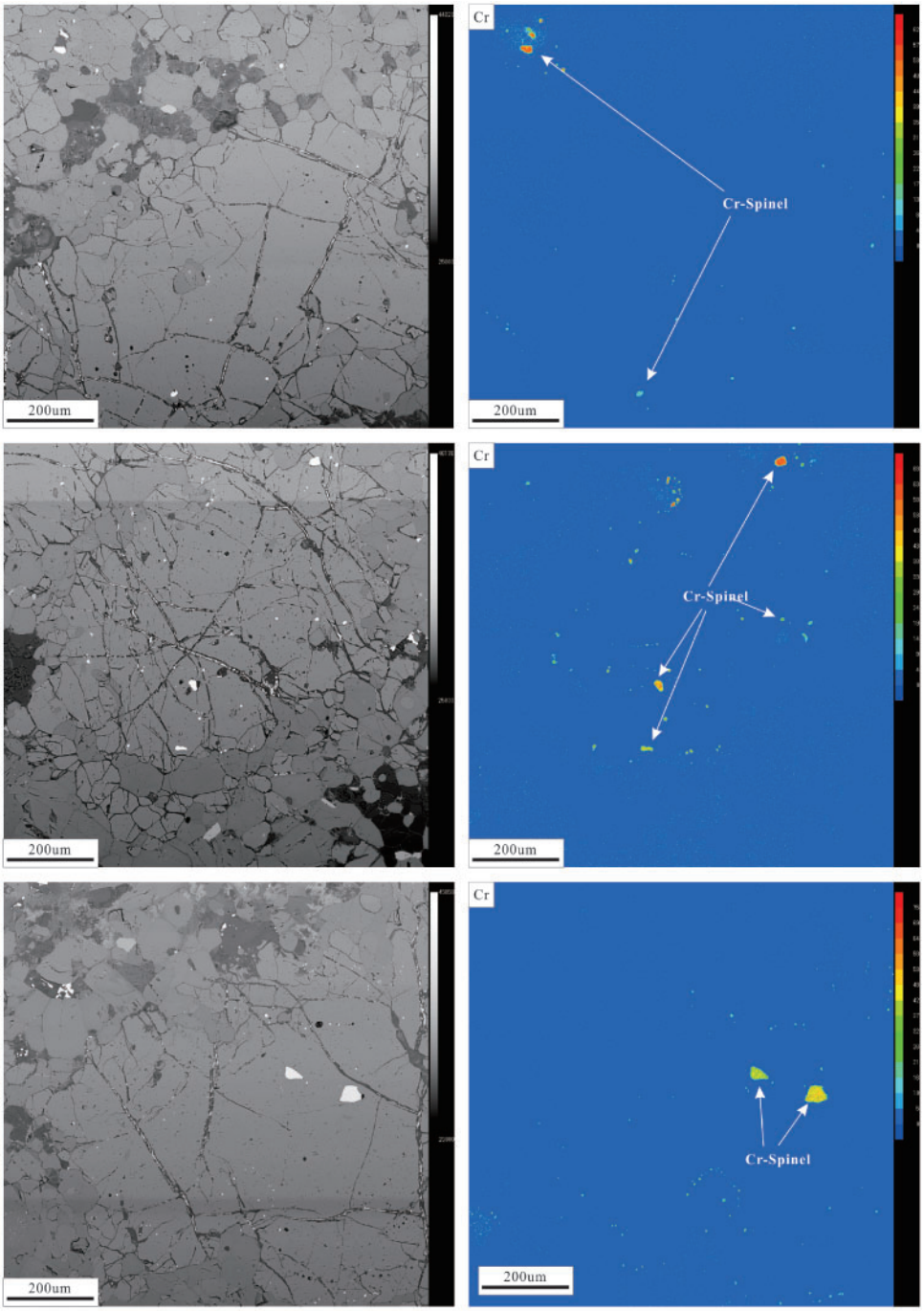

Fig. 4

Fig. 4. BSE image and WDS Cr map showing the variation of Cr content in Cr-spinels hosted in individual olivine phenocrysts.

(Qi *et al.*, 2004). Ten grams of rock powder and the appropriate amount of isotope spike solution containing ^{193}Ir, ^{101}Ru, ^{194}Pt and ^{105}Pd were digested with 30 ml HF in a 120 ml PTFE beaker. The solutions were then evaporated to dryness before a 5 ml HF + 15 ml HNO_3 mixture was added and the sample was digested for 48 h at ~190°C. The PGE within the final solution were then collected using a Te-coprecipitation approach (Qi *et al.*, 2004).

Whole-rock Rb–Sr and Sm–Nd isotopic compositions were determined by multicollector (MC)–ICP–MS employing a Nu Plasma II instrument at the State Key Laboratory of Environmental Geochemistry, Institute of Geochemistry, Chinese Academy of Sciences, Guiyang, China. Prior to analysis, ~100 mg aliquots of sample powder were dissolved in closed Teflon beakers using a mixed HF–HNO_3–$HClO_4$ acid solution. Sr and Nd were extracted using AG50W-X12 cation-exchange resin and

P507 extraction chromatography resin, respectively. Mass fractionation corrections for Sr and Nd isotopic ratios were based on $^{86}Sr/^{88}Sr = 0{\cdot}1194$ and $^{146}Nd/^{144}Nd = 0{\cdot}7219$, respectively. Repeat analysis of the Sr and Nd standards NIST-987 and JNdi-1 yielded ratios of $0{\cdot}710261 \pm 0{\cdot}00005$ (2σ, $n = 10$) and $0{\cdot}5120665 \pm 0{\cdot}000005$ (2σ, $n = 8$), respectively. The analysis of the BCR-2 standard during this study yielded $^{87}Sr/^{86}Sr$ and $^{143}Nd/^{144}Nd$ ratios of $0{\cdot}704990 \pm 0{\cdot}000006$ (2σ) and $0{\cdot}512601 \pm 0{\cdot}000005$ (2σ), respectively and initial isotopic ratios were determined using Rb, Sr, Sm and Nd concentrations that were analysed by ICP–MS.

RESULTS

Mineral chemistry

The measured compositions of the olivine and Cr-spinel within the chilled marginal rocks of the Panzhihua intrusion are given in the Supplementary Data; supplementary data are available for downloading at http://www.petrology.oxfordjournals.org. The forsterite (Fo = $100 \times MgO/(MgO + FeO)$ in molar proportions) contents of the olivine in the chilled marginal rocks range from 71 to 83 (Fig. 5a, b). The most primitive olivine (Fo_{83}) is close to the most primitive olivine (Fo_{81}) within the overlying layered series of the intrusion (Pang *et al.*, 2009; Song *et al.*, 2013). The olivine within the chilled marginal rocks contains <0·4 wt % MnO, similar to the olivine within the overlying layered series in the Panzhihua intrusion. The negative correlation between MnO concentration and Fo content for olivine within the chilled marginal rocks plots within the fractional differentiation trend defined by the compositions of olivine from high-Ti picrites and mafic–ultramafic intrusions within the ELIP (Fig. 5a), suggesting that these olivines crystallized from magma undergoing differentiation. The positive correlation between NiO concentration and Fo content for these olivines also matches the fractional differentiation trend of olivines within high-Ti ELIP picrites and the Xinjie intrusion (Fig. 5b). However, the olivine within the chilled marginal rocks has NiO contents that are significantly higher than those of olivine within the overlying layered series in the Panzhihua intrusion. The Cr-spinel inclusions within olivine in the chilled marginal rocks contain 8–30 wt % Cr_2O_3. The Mg# of Cr-spinel from the chilled marginal rocks are less than 0.2, much lower than those from the coeval high-Ti picrites (Fig. 5c, d). The high-Ti picrites show a positive correlation between Fo contents of olivine and Mg# as well as Cr_2O_3 contents in Cr-spinel (Fig. 5d, e), consistent with fractional crystallization. However, such correlations are not observed in the samples from the chilled marginal zone. In fact, the Cr_2O_3 content and Cr# of Cr-spinels is highly variable within individual olivines (e.g. Cr_2O_3 contents of 8–30 wt% from sample PZH1302; Figs 4, 5e, f). Such wide variations are often due to variable reaction with unequilibrated liquid during slow cooling (Roeder & Campbell, 1985). In contrast, the rapidly cooled Emeishan picrites preserve the composition of fractional crystallization. Thus, the compositions of coexisting olivine and spinel from the Emeishan picrites (Kamenetsky *et al.*, 2012) were used to estimate the fO_2 of the Emeishan basaltic magma. The fO_2 of high-Ti picrites from the Yongsheng area and low-Ti picrites from the Dali area are FMQ + 1 to ~ FMQ + 2·5 and around FMQ (FMQ=fayalite–magnetite–quartz), respectively. This suggests that the high-Ti series are more oxidized than the low-Ti series in the Emeishan LIP.

Whole-rock major and trace element compositions

The whole-rock major and trace element compositions of the chilled marginal microgabbros and olivine–phyric gabbros are given in Table 1. The TiO_2, $Fe_2O_3^T$, Al_2O_3 and SiO_2 concentrations of the chilled marginal samples show negative correlations with their MgO contents (Fig. 6). The microgabbros contain 45·1–46·1 wt % SiO_2, 8·0–8·7 wt % MgO, 11·2–13·3 wt % Al_2O_3, 12·2–14·4 wt % $Fe_2O_3^T$ and 10·6–13·0 wt % CaO (Fig. 6). These samples have TiO_2 contents (2·6–2·8 wt %) that are higher than those of the low-Ti ELIP basalts, but lower than the maximum value the high-Ti basalts (5 wt %). In fact, these concentrations are close to the lower end of the TiO_2 concentrations within the high-Ti ELIP basalts (2·5 wt %). The microgabbros are also compositionally similar to the average Emeishan HT2 basalts (especially in terms of TiO_2 content) in the neighboring Ertan area, 20 km north of the Panzhihua intrusion. The olivine–phyric gabbros have lower concentrations of SiO_2, Al_2O_3, TiO_2, CaO and $Na_2O + K_2O$, and higher concentrations of MgO than the microgabbros (Table 1; Fig. 6). The MgO contents of these samples are up to 30 wt %, higher than the estimated MgO content of the primary ELIP magma (MgO = ~23 wt %; Xu & Chung, 2001; Zhang *et al.*, 2006; Hanski *et al.*, 2010; Li *et al.*, 2012; Ren *et al.*, 2017), suggesting that these olivine–phyric gabbros record olivine accumulation processes.

The chilled marginal rocks of the Panzhihua intrusion contain 260–2310 ppm Cr, 150–385 ppm V and 95–1510 ppm Ni. The Cr and Ni contents of these samples show positive correlations with MgO, whereas V concentrations show a negative correlation with MgO content (Fig. 7). The olivine–phyric gabbros have higher concentrations of Cr and Ni than the microgabbros, which is consistent with the observation that Cr and Ni are compatible in Cr-spinel and olivine, respectively. There is no positive correlation between the Cu and MgO concentrations of samples from the chilled marginal rocks and the microgabbros have lower Cu contents (Fig. 7d) than olivine-hosted melt inclusions within the high-Ti picrites of the ELIP (Kamenetsky *et al.*, 2012). All of the chilled marginal rocks have chondrite-normalized rare earth element (REE) patterns that are

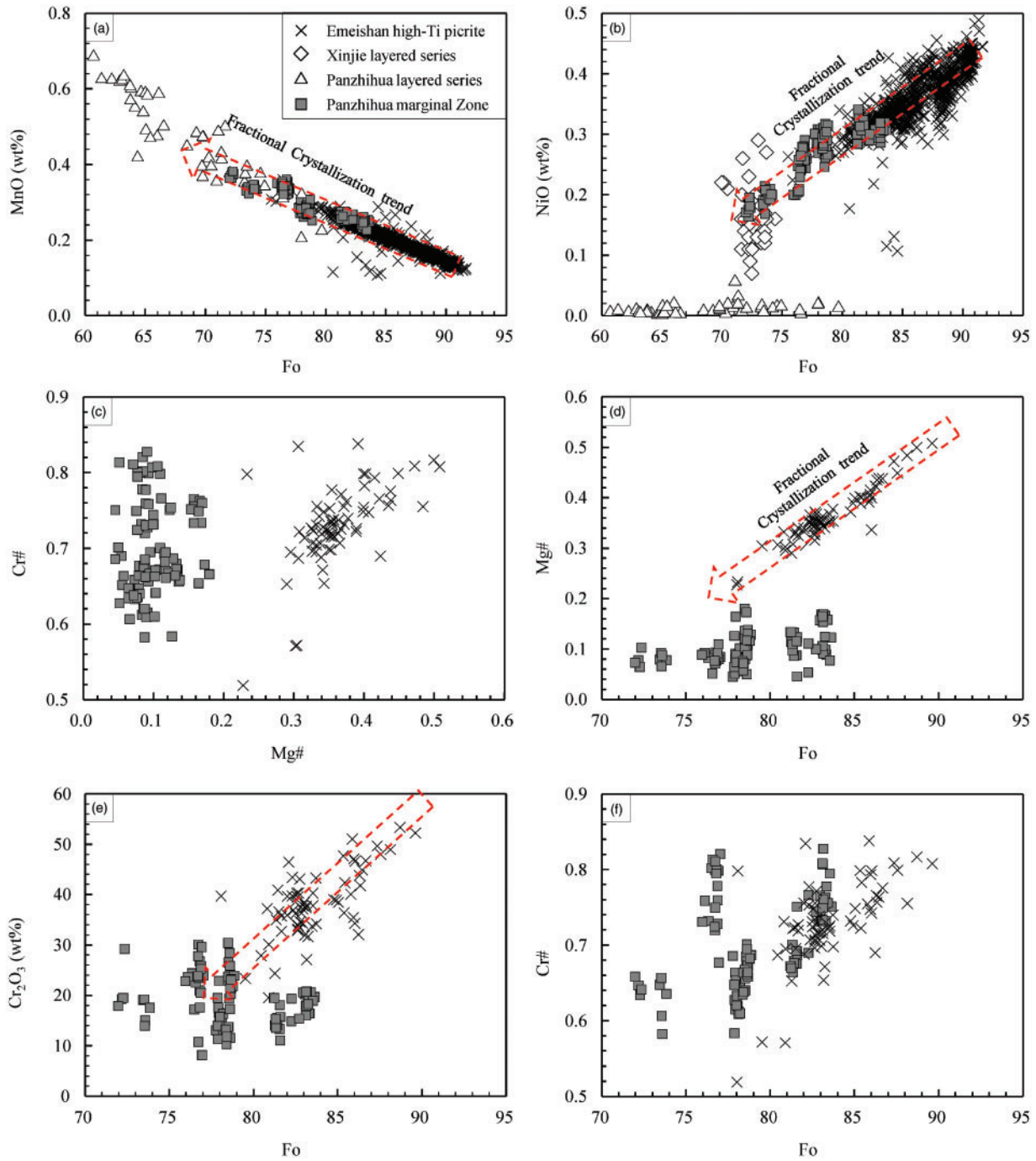

Fig. 5. Compositional variation in olivine and Cr-spinel in the Marginal Zone of the Panzhihua intrusion. (a, b) Mn and Ni in olivine vs Fo of olivine. (c) Cr# vs Mg# of Cr-spinel; (d–f) Mg#, Cr_2O_3 and Cr# of Sr-spinel vs Fo content of olivine. Compositions of Emeishan high-Ti picrites are from Kamenetsky *et al.* (2012), Tao *et al.* (2015) and Yu *et al.* (2017). The compositions of olivine from the layered series of the Panzhihua (Pang *et al.*, 2009) and Xinjie (Wang *et al.*, 2007) intrusions are shown in the same diagrams for comparison with the Marginal Zone.

enriched in light REE (LREE) relative to the heavy REE (HREE; Fig. 8). The microgabbros also have similar REE concentrations and patterns to the Emeishan HT2 basalts from the Ertan area. The olivine–phyric gabbros have lower concentrations of the REE than the microgabbros. This reflects an olivine dilution effect, as the REE are incompatible in olivine.

Chalcophile elements

The chilled marginal rocks within the Panzhihua intrusion have variable S contents (<0·01 to 1·48 wt %; Table 1), with the high S concentrations suggesting that some of these samples record sulfide accumulation processes. In comparison, the low S contents (e.g. <0·1 wt %) of some samples may reflect the loss of S

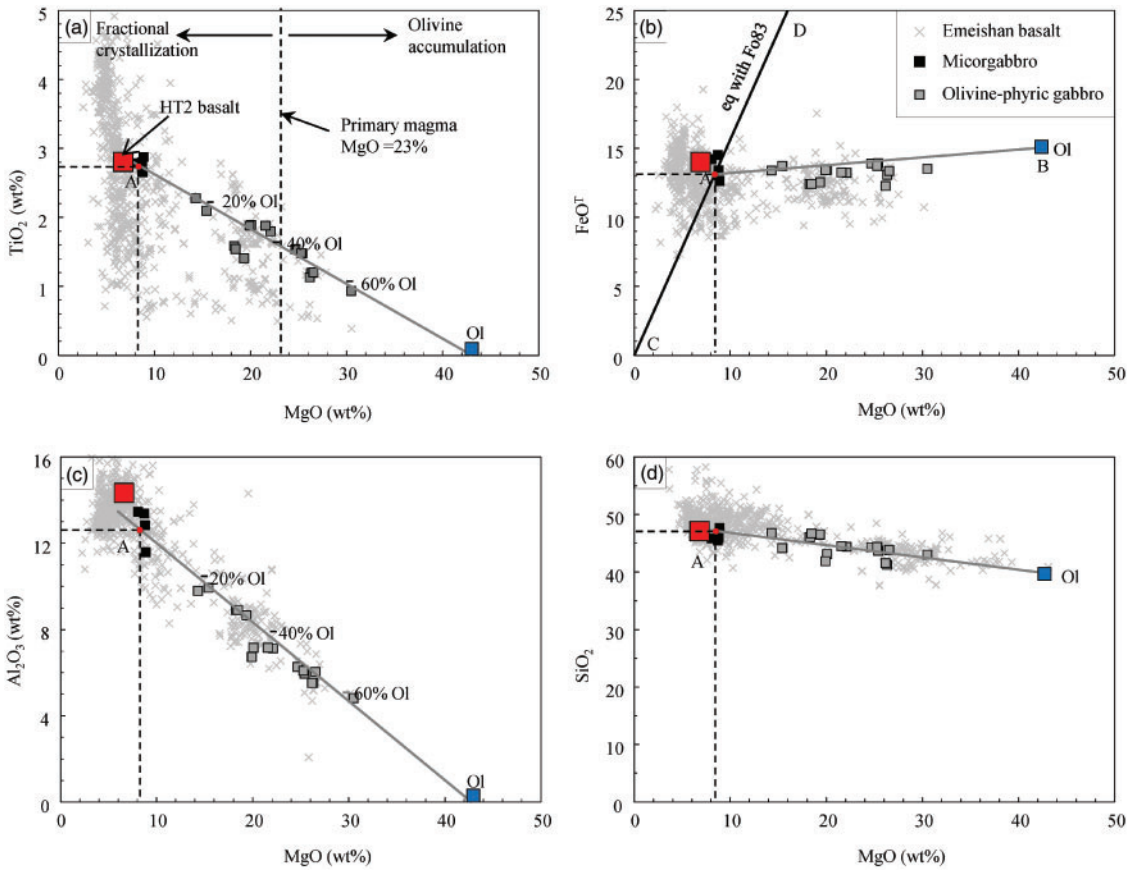

Fig. 6. Variations of (a)TiO_2, (b) FeO^T, (c) Al_2O_3 and (d) SiO_2 vs whole-rock MgO for the Marginal Zone of the Panzhihua intrusion. The data for Emeishan basalts are from GEOROC: (http://georoc.mpch-mainz.gwdg.de/georoc). The data for Emeishan HT2 basalts and MgO contents of primary magmas are from Xu *et al.* (2001) and Ren *et al.* (2017), respectively. The FeO/FeO^T of the magmas in Fig. 6b is adjusted for the FMQ + 1 buffer using the MELTS program of Ghiorso & Sack (1995). The line C to D indicates liquid compositions in equilibrium with olivine of Fo83 using the Mg–Fe olivine-liquid partition coefficient of 0·34 from Matzen *et al.* (2011). Ol has the most primitive composition (Fo83) in the olivine–phyric gabbros. Point A represents the estimated parental magma composition for the olivine–phyric gabbros.

during post-magmatic hydrothermal alteration, as olivine-hosted melt inclusions within the Emeishan high-Ti picrites have maximum S contents of 0·18 wt % (Kamenetsky *et al.*, 2012). These samples contain highly variably PGE concentrations with total PGE contents of 8·6–32·9 ppb. The IPGE (Os, Ir and Ru) are strongly partitioned into spinel (Brenan *et al.*, 2012), which explains why the Ir (0·73–2·33 ppb) and Ru (1·26–3·40 ppb) contents of the olivine–phyric gabbros are much higher those of the microgabbros (0·31–0·40 ppb Ir, 0·11–0·64ppb Ru), although both sets of samples have similar PPGE (Rh, Pt and Pd) contents (Fig. 9 and Table 2). These samples have highly variable Cu/Pd ratios (0·75–$3{\cdot}44 \times 10^4$) that show broadly negative correlations with their Pd contents (Fig. 10). The Cu/Pd ratios of most samples are higher than mantle values (10^3–10^4 range, with median values of 5488; Barnes *et al.*, 2015) and the lower end of the coeval high-Ti basalts (Fig. 10), suggesting that these samples record early sulfide removal. The samples plot within the lower part of the PGE-depleted field in the Cu/Pd–Pd diagram, which is defined by the overlying Panzhihua layered series and other mafic–ultramafic layered intrusions within the ELIP, but contrasts sharply with the PGE-undepleted Xinjie intrusion, which also forms part of the ELIP.

Whole-rock Sr–Nd isotopes

The Rb–Sr and Sm–Nd isotopic compositions of the chilled marginal rocks of the Panzhihua intrusion are given in Table 3. These rocks have relatively constant initial $^{87}Sr/^{86}Sr$ (0·7043 to 0·7054) but large variations in ε_{Nd} (-1·49 to +4·18) values (t = 259 Ma; Fig. 11). In general, the olivine–phyric gabbros are characterized by depleted Nd isotopic compositions (+1·15 to +4·18) that overlap with the values of the overlying Panzhihua layered series (Zhang *et al.*, 2009; Howarth & Prevec, 2013; Song *et al.*, 2013), the Emeishan HT2 basalts from the Ertan area (Xu *et al.*, 2001) and the Emeishan picrites (Zhang *et al.*, 2006; Li *et al.*, 2012). The initial $^{87}Sr/^{86}Sr$ ratios of the microgabbros (0·7045 to 0·7054) are similar to the values of the olivine–phyric gabbros (0·7043–0·7052). However, the microgabbros have more enriched Nd isotopic compositions (-1·49 to +0·06) than the olivine–phyric gabbros (+1·15 to +4·18).

Table 1: Major (wt %) and trace element (ppm) concentrations of rocks from the Marginal Zone of the Panzhihua intrusion

Sample	PZH1305	PZH1307	PZH1309	PZH1310	PZH1301	PZH1302	PZH1303	PZH1304	PZH1405	PZH1406
Rock type	GB	GB	GB	GB	OGB	OGB	OGB	OGB	OGB	OGB
SiO_2	46·1	45·1	45·4	45·2	43·2	42·9	42·6	41·5	44·50	44·98
TiO_2	2·78	2·60	2·76	2·78	1·75	1·81	1·17	0·90	1·53	1·36
Al_2O_3	11·20	12·60	13·35	13·30	6·93	6·90	5·87	4·65	8·60	8·37
Cr_2O_3	0·08	0·04	0·04	0·05	0·24	0·24	0·31	0·35	0·21	0·23
Fe_2O_3	12·22	13·16	14·08	14·42	12·86	12·77	12·99	13·04	12·00	12·12
MnO	0·18	0·26	0·22	0·22	0·17	0·17	0·17	0·17	0·17	0·17
MgO	8·59	8·61	8·00	8·65	21·5	20·8	25·8	29·4	17·65	18·70
CaO	10·60	13·05	12·45	11·95	7·91	7·94	6·69	5·14	8·22	8·09
Na_2O	4·31	2·13	2·33	2·32	2·06	2·15	1·38	1·16	0·95	1·36
K_2O	0·43	0·31	0·21	0·22	0·75	0·84	0·41	0·42	2·81	1·38
P_2O_5	0·25	0·30	0·31	0·30	0·16	0·16	0·11	0·08	0·14	0·13
S	0·02	0·01	0·00	0·01	0·02	0·04	0·02	0·02	0·17	0·16
LOI	3·05	0·91	0·61	0·58	1·81	2·39	1·68	2·98	3·61	2·46
Total	99·79	99·07	99·76	99·99	99·34	99·07	99·18	99·79	100·39	99·35
Sc	36·5	33·7	35·6	36·0	24·2	23·5	21·3	17·6	21·5	23·3
V	385	349	342	366	250	260	194	152	284	272
Cr	557	260	280	306	1620	1660	2100	2310	1092	1210
Co	48·8	47·1	50·8	53·1	92·0	91·5	103·0	115·0	67·6	74·7
Ni	102	95	100	107	1080	1070	1270	1510	705	747
Cu	129	109	123	182	93·4	74·7	66·1	11·2	65·6	64·8
Zn	113	117	132	139	101	97·9	101	101	110	106
Ga	16·4	19·8	17·7	19·3	12·1	12·3	10·1	8·13	15·0	13·9
Rb	13·6	3·96	0·93	0·75	15·6	14·2	8·41	17·3	142·0	43·5
Sr	204	591	559	669	361	382	188	118	152	215
Y	25·2	25·1	26·1	27·9	16·2	17·0	12·4	9·6	18·1	16·5
Zr	177	112	113	125	118	122	72·5	55·5	93·5	85·4
Nb	28·6	27·5	29·8	30·7	13·6	14·0	10·7	8·33	14·7	13·3
Ba	142	156	269	283	172	178	132	96	240	208
La	29·4	19·5	21·9	23·5	12·3	13·0	9·17	7·21	12·3	10·7
Ce	65·0	48·8	55·0	59·6	29·0	30·5	20·2	15·8	27·8	24·4
Pr	7·91	6·60	7·30	7·90	3·82	4·01	2·54	1·97	3·49	3·05
Nd	33·1	30·6	32·9	35·3	17·4	17·9	11·5	8·8	14·9	13·5
Sm	6·90	6·88	7·17	7·57	4·03	4·25	2·80	2·20	3·72	3·33
Eu	2·26	2·35	2·50	2·62	1·43	1·48	1·05	0·77	1·11	1·07
Gd	6·42	6·05	6·60	7·07	3·99	4·13	2·92	2·12	3·69	3·33
Tb	0·96	0·92	0·97	1·05	0·61	0·63	0·45	0·33	0·66	0·63
Dy	4·97	4·92	5·06	5·42	3·23	3·36	2·44	1·85	3·71	3·27
Ho	0·89	0·87	0·96	1·00	0·59	0·61	0·44	0·34	0·72	0·62
Er	2·43	2·40	2·57	2·66	1·52	1·59	1·16	0·89	1·88	1·65
Tm	0·30	0·30	0·34	0·35	0·19	0·20	0·15	0·12	0·24	0·24
Yb	1·81	1·92	2·07	2·14	1·18	1·25	0·94	0·72	1·41	1·36
Lu	0·25	0·26	0·28	0·31	0·17	0·17	0·14	0·09	0·21	0·20
Hf	4·55	3·13	3·24	3·56	3·02	3·03	1·89	1·38	2·64	2·46
Ta	1·46	1·28	1·38	1·40	0·77	0·77	0·61	0·47	0·92	0·85
Pb	4·03	1·20	1·57	1·76	2·89	2·23	1·55	1·14	7·09	5·28
Th	4·26	0·15	0·17	0·12	1·34	1·32	1·20	1·14	1·64	1·40
U	0·94	0·11	0·05	0·04	0·42	0·48	0·30	0·27	0·84	0·35

Sample	PZH1407	PZH1408	PZH1409	PZH1410	PZH1411	PZH1412	PZH1413	PZH1414	PZH1416	PZH1417
Rock type	OGB	OGB	OGB	OGB	OGB	OGB	OGB	OGB	OGB	OGB
SiO_2	45·43	41·51	41·02	42·95	43·24	42·85	43·69	45·97	39·69	39·24
TiO_2	1·50	1·82	1·84	2·04	1·50	1·45	1·46	2·24	1·15	1·07
Al_2O_3	8·67	6·88	6·60	9·66	6·12	5·83	6·00	9·62	5·31	5·21
Cr_2O_3	0·21	0·23	0·23	0·17	0·29	0·30	0·30	0·15	0·30	0·31
Fe_2O_3	12·08	12·93	13·14	13·34	13·58	13·64	13·52	13·15	12·58	11·58
MnO	0·18	0·18	0·18	0·19	0·19	0·19	0·19	0·19	0·19	0·23
MgO	17·95	19·31	19·50	15·00	24·1	24·9	24·9	14·05	25·3	24·7
CaO	8·77	10·25	13·60	9·80	7·02	7·25	6·87	9·65	10·30	12·15
Na_2O	1·24	1·50	1·14	1·79	1·26	1·32	1·24	2·27	0·26	0·15
K_2O	1·33	1·54	0·42	2·33	0·49	0·46	0·46	0·89	1·28	0·03
P_2O_5	0·14	0·30	0·56	0·18	0·13	0·14	0·13	0·22	0·09	0·05
S	0·06	0·65	0·30	0·13	0·09	0·07	0·05	0·03	0·51	1·48
LOI	2·43	2·32	2·01	2·28	1·81	1·68	1·29	1·05	2·82	5·17
Total	99·93	98·77	100·24	99·73	99·73	100·01	100·05	99·45	99·27	99·89
Sc	0·0	22·3	25·7	28·5	21·2	20·3	22·1	26·9	17·7	18·2
V	282	302	330	334	219	215	220	303	199	150
Cr	1130	1304	1311	921	1410	1430	1480	706	1500	1550
Co	73·9	83·0	80·0	71·6	91·8	96·1	96·5	65·9	96·6	83·1

(continued)

Table 1: Continued

Sample	PZH1407	PZH1408	PZH1409	PZH1410	PZH1411	PZH1412	PZH1413	PZH1414	PZH1416	PZH1417
Ni	704	829	787	616	1030	1120	1110	492	1160	1190
Cu	110	159	107	87·8	112	180	72·4	174	81·8	83·5
Zn	103	113	107	114	114	113	114	111	108	104
Ga	15·3	15·0	13·8	16·0	11·1	10·2	10·8	17·0	9·69	10·1
Rb	42·9	49·5	10·9	82·4	10·7	9·30	9·87	17·3	36·8	1·37
Sr	198	414	438	341	207	227	240	668	135	49
Y	17·5	17·4	18·8	19·9	13·1	13·0	12·9	20·7	11·5	12·1
Zr	90·3	138	125	139	107	99·8	106	175	81·2	75·7
Nb	8·30	23·3	30·9	16·7	12·6	13·3	12·6	23·5	17·3	9·19
Ba	158	553	240	551	176	154	147	442	664	24
La	11·8	22·0	21·5	17·7	14·0	14·2	13·9	25·0	9·65	6·05
Ce	27·0	43·4	43·8	39·0	31·1	31·3	31·1	54·4	23·4	16·5
Pr	3·30	5·42	5·53	5·20	4·00	4·02	4·03	7·15	3·26	2·61
Nd	14·5	21·9	24·0	22·6	17·1	17·6	17·2	29·2	14·4	11·9
Sm	3·60	4·98	4·96	4·97	3·62	3·75	3·51	6·07	3·15	2·69
Eu	1·07	1·45	1·55	1·75	1·20	1·17	1·18	1·96	0·99	0·86
Gd	3·81	4·19	4·50	4·93	3·63	3·62	3·26	5·78	2·88	2·65
Tb	0·63	0·69	0·75	0·80	0·51	0·52	0·53	0·83	0·43	0·43
Dy	3·54	3·46	4·22	4·21	2·73	2·61	2·71	4·42	2·33	2·32
Ho	0·66	0·69	0·69	0·87	0·52	0·52	0·49	0·82	0·46	0·42
Er	1·73	1·68	1·77	2·10	1·33	1·37	1·29	2·08	1·20	1·15
Tm	0·24	0·23	0·26	0·28	0·17	0·18	0·17	0·29	0·17	0·17
Yb	1·41	1·40	1·40	1·61	0·93	1·01	0·98	1·64	0·92	0·96
Lu	0·20	0·18	0·22	0·23	0·14	0·14	0·14	0·22	0·11	0·13
Hf	2·47	4·12	3·45	3·77	2·58	2·44	2·62	4·41	2·11	1·88
Ta	0·67	1·22	1·36	1·17	0·87	0·83	0·88	1·66	0·76	0·69
Pb	4·15	6·78	7·56	9·90	1·51	2·67	1·34	3·79	5·27	2·14
Th	1·44	2·47	2·73	1·35	1·75	1·24	1·85	3·62	1·07	0·91
U	0·47	1·26	1·32	0·26	0·49	0·27	0·44	0·73	0·49	0·27

GB, Microgabbro; OGB, olivine–phyric gabbro.

DISCUSSION

Petrogenesis of the chilled marginal rocks of the Panzhihua intrusion

The chilled marginal rocks of the Panzhihua intrusion contain petrographically and compositionally contrasting microgabbro and olivine–phyric gabbro units. The fine-grained and equigranular textures of the microgabbros (Fig. 3b) are consistent with the rapid nucleation and cooling processes that are similar to some of those recorded within the marginal zones of the Bushveld Complex and the Skaergaard intrusion (Hoover, 1989; Barnes *et al.*, 2010; Maier *et al.*, 2016) as well as the intra-plutonic quench zones of the Kap Edvard Holm layered gabbro complex (Tegner *et al.*, 1993). Combining this observation with the highly incompatible element contents of these samples, we infer that the microgabbros represent a quench zone where magmas were chilled against the wall rocks during emplacement along the floor of a magma chamber. The similarities between the major and trace compositions of these microgabbros and the coeval Emeishan basalts (Figs 6–8) also suggest that the former may record melt compositions. The olivine–phyric gabbros have a fine-grained matrix that is mineralogically similar to the microgabbros and contain abundant coarse-grained olivines. The bulk compositions of these olivine–phyric gabbros can be reproduced by mixing the compositions of the fine-grained microgabbros with variable proportions (20%–60%) of olivine (Fig. 6). The linear correlations defined by the major and trace element compositions of these units in binary diagrams (Figs 6, 7) as well as the similar trace element patterns of these two units (Fig. 8), suggest that the microgabbros and the olivine–phyric gabbros are comagmatic. Olivine–phyric gabbros have also been found in numerous other mafic sills, including the Palisades sill in eastern North America (Gorring & Naslund, 1995; Haddad & Naslund, 2017), the Shiant Isles Main Sill in NW Scotland (Gibb & Henderson, 2006; Holness *et al.*, 2017) and the Franklin Sill in Arctic Canada (Hayes *et al.*, 2015*a*, 2015*b*).

There are a number of proposed models for the formation of these olivine–phyric gabbros within the chilled margin of mafic intrusions, including: (1) *in situ* derivation by the isochemical crystallization of picritic liquids; (2) formation as cumulates from mafic liquids that fractionated *in situ*; and (3) derivation from olivine-laden magma slurries. The composition of the primary magma for the Emeishan picrites has been estimated using various methods (Xu & Chung, 2001; Zhang *et al.*, 2006; Hanski *et al.*, 2010; Li *et al.*, 2012; Ren *et al.*, 2017), all of which suggest that this primary magma contained ~23 wt % MgO. However, the olivine–phyric gabbros contain up to 30 wt % MgO and, therefore, cannot have formed by the *in situ* isochemical crystallization of a picritic magma. This excess MgO content is consistent with a scenario in which these olivine–phyric gabbros formed as cumulates from mafic liquids that fractionated *in situ*. Olivine compositional variations within these units (Fo_{83} to Fo_{71}) may also be consistent with

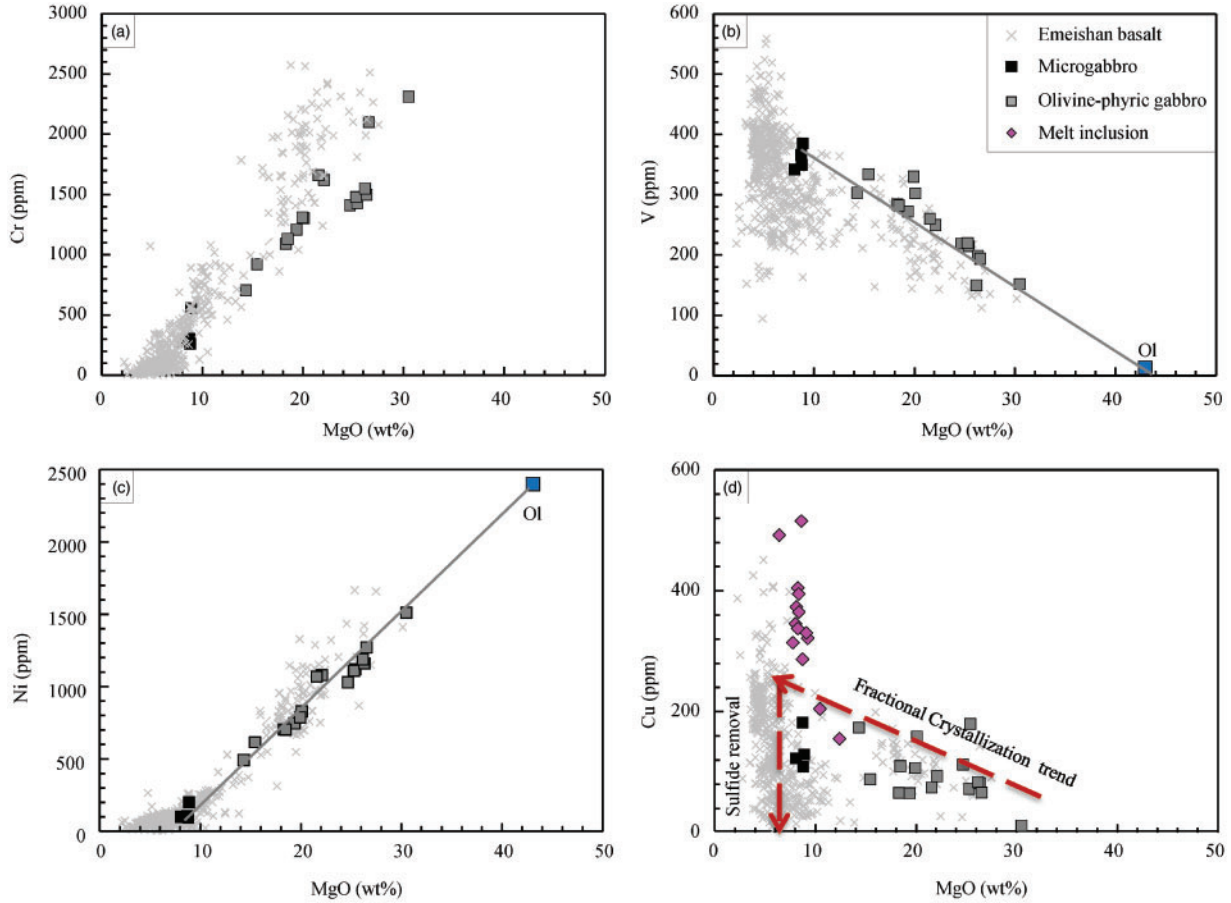

Fig. 7. Variations of (a) Cr, (b)V, (c) Ni and (d) Cu vs whole-rock MgO for the Marginal Zone of the Panzhihua intrusion. Ol has the most primitive composition of Fo83 in the olivine–phyric gabbros. The data for the Emeishan basalts are from GEOROC: (http://georoc.mpch-mainz.gwdg.de/georoc). The Cu contents of melt inclusion hosted in olivine are from Kamenetsky *et al.* (2012).

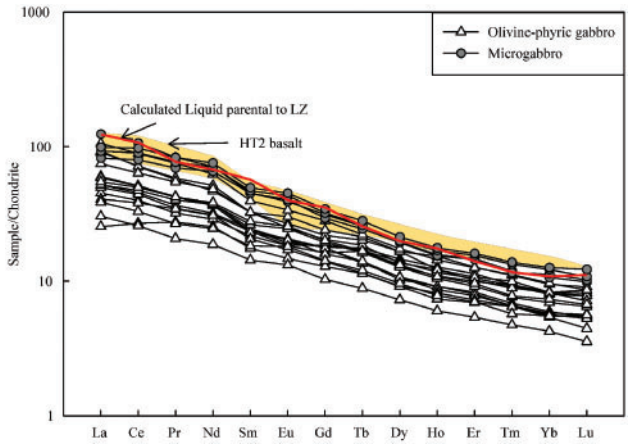

Fig. 8. Chondrite normalized rare earth element (REE) patterns for the marginal rocks of the Panzhihua intrusion. Red line is the liquid trace element composition calculated using the average composition of clinopyroxene from the lower ore-bearing zone of the Panzhihua intrusion and the Cpx/liquid partition coefficients of Hill *et al.* (2000). The data for Emeishan HT2 basalts are from Xu *et al.* (2001). Normalization values are from McDonough & Sun (1995).

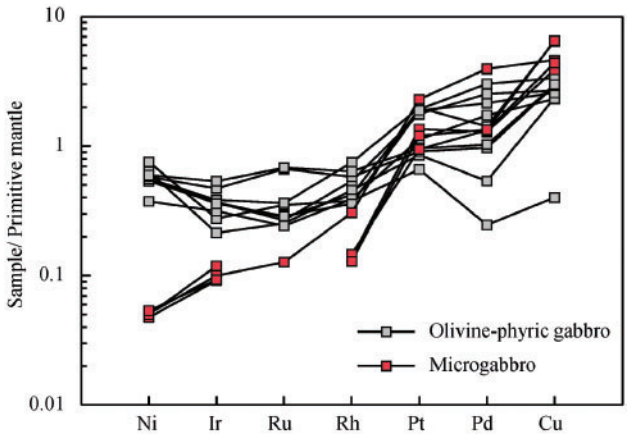

Fig. 9. Primitive mantle-normalized chalcophile element patterns for marginal rocks from the Panzhihua intrusion. The normalization values are from Barnes & Maier (1999).

closed-system fractional crystallization of a single pulse of magma. However, this scenario cannot explain the textural observations from the study area, as the presence of a fine-grained matrix indicates that the

Table 2: PGE (ppb), Ni and Cu (ppm) concentrations for the Marginal Zone of the Panzhihua intrusion and reference material WGB-1

Sample	Rock type	Ni	Ir	Ru	Rh	Pt	Pd	Cu	Cu/(Pd × 10^4)
PZH1305	GB	102	0·34	0·64	0·29	16·04	15·67	129	0·82
PZH1307	GB	95	0·31	0·14	0·13	9·45	5·10	109	2·14
PZH1309	GB	100	0·40	0·22	0·14	6·60	5·26	123	2·34
PZH1310	GB	107	0·32	0·11	0·12	8·40	5·29	182	3·44
PZH1301	OGB	1080	1·11	1·45	0·48	12·27	7·86	93·.4	1·19
PZH1301		1·25	1·40	0·40	13·40	7·95			
PZH1302	OGB	1070	1·24	1·34	0·51	12·32	10·02	74·7	0·75
PZH1303	OGB	1270	0·73	1·26	0·43	5·.97	2·13	66·1	3·10
PZH1304	OGB	1510	0·94	1·75	0·36	4·63	0·98	11·2	1·15
PZH1406	OGB	747	1·07	1·21	0·37	7·89	6·85	64·8	0·95
PZH1412	OGB	1120	1·30	1·81	0·71	13·.82	5·62	179·88	3·20
PZH1413	OGB	1110	2·33	1·40	0·35	13·32	7·46	72·40	0·85
PZH1416	OGB	1160	1·60	3·33	0·55	6·35	3·88	81·84	2·11
PZH1417	OGB	1190	1·82	3·40	0·61	6·72	4·09	83·53	2·04
WGB-1	Measured		0·24	0·21	0·1	4·50	12·41		
WGB-1	Certified		0·33	0·3	0·31	6·10	13·9		
Blank			<0·01	0·02	<0·01	0·02	0·03		

olivine–phyric gabbros also cooled and nucleated relatively rapidly, suggesting that it would have been difficult to crystallize coarse-grained (1–5 mm) olivine *in situ* (Fig. 3). The unusual characteristic of the olivine–phyric gabbros is the wide variations in Cr_2O_3 content of Cr-spinel within each individual sample (Fig. 5). Such variations cannot be attributed to subsolidus exsolution, since there is no sign of exsolution in the grain (Fig. 5e). Roeder & Campbell (1985) suggested that chromite within olivine can equilibrate and exchange elements with surrounding liquid through the olivine. The possible mechanisms include elements such as Cr, Al, Ti and Fe^{3+} diffusing through the olivine structure or the enclosed Cr-spinel maintains direct contact with the liquid along fine fractures. Such a process only occurs in slowly cooled large intrusive complexes where the liquid has a greater opportunity to equilibrate with the early minerals. Rapidly cooled volcanic rocks and small intrusions have little opportunity to react with the cooling liquid and thus preserve the composition of fractional crystallization (Roeder & Campbell, 1985). As a result, the lack of a positive correlation between the Cr_2O_3 contents of the Cr-spinel inclusions and the Fo contents of their host olivine, and the wide variations of Cr content in Cr-spinel inclusions within individual olivines, could be due to the reaction between Cr-spinel and unequilibrated magma at depth, since the olivine–phyric gabbros were formed by rapidly cooling in Panzhihua magma chamber.

The olivine–phyric gabbros are texturally similar to picrites and ultramafic dikes within the ELIP, both of which contain olivine phenocrysts that formed by primary magma differentiation in a deep-seated magma chamber and were then transported to the surface or shallow crust by differentiated melts (Kamenetsky *et al.*, 2012; Wang *et al.*, 2014; Munteanu *et al.*, 2017). This suggests that the magmas that formed the olivine–phyric gabbros in the chilled marginal rocks were emplaced as olivine-laden magma slurries that were generated in a staging magma chamber at depth. A similar model has been proposed for the generation of the marginal zones of large layered intrusions such as the Bushveld Complex in South Africa (Wilson, 2012, 2015), the Doros layered intrusion in Namibia (Owen-Smith & Ashwal, 2015) and small mafic sills such as the Palisades sill in eastern North America (Gorring & Naslund, 1995; Haddad & Naslund, 2017), the Shiant Isles Main Sill in NW Scotland (Gibb & Henderson, 2006; Holness *et al.*, 2017) and the Franklin Sill in Arctic Canada (Hayes *et al.*, 2015*a*, 2015*b*). The large variations in the Cr contents of the olivine-hosted Cr-spinel inclusions within these units indicate that the olivines and Cr-spinel formed as a result of multiple generations of crystallization and re-equilibration with liquid at depth. We suggest that the transported magma captured olivine from an olivine crystal mush within a deep magma chamber. This olivine crystallized from another batch of magma before being captured by the transporting magma and being emplaced along the floor of the Panzhihua magma chamber. The variations in the proportion of olivine within the chilled marginal rocks of the Panzhihua intrusion reflect variations in the settling of olivine phenocrysts prior to solidification.

The Nd isotopic compositions of microgabbros ($\varepsilon_{Nd}(t)$=-1·49 to +0·06) are more enriched than the overlying olivine–phyric gabbros ($\varepsilon_{Nd}(t)$= +1·15 to +4·18, Fig. 11) and the layered series of the Panzhihua intrusion. A similar feature of upward gradational depletion in Nd isotope composition has also been identified in the marginal zone of the Jianshan section (Howarth & Prevec, 2013). Such variation of isotopic compositions in layered intrusions has been interpreted as less contamination by wall rocks away from margin of the intrusion (Sorensen & Wilson, 1995). Ganino *et al.* (2013) proposed that the Panzhihua intrusion experienced 8–13% assimilation of the high $\delta^{18}O$ ($\delta^{18}O_{Dol}$=24·6–28·6‰) dolomite footwall rocks. However, Yu *et al.* (2015) obtained the oxygen isotopic compositions of

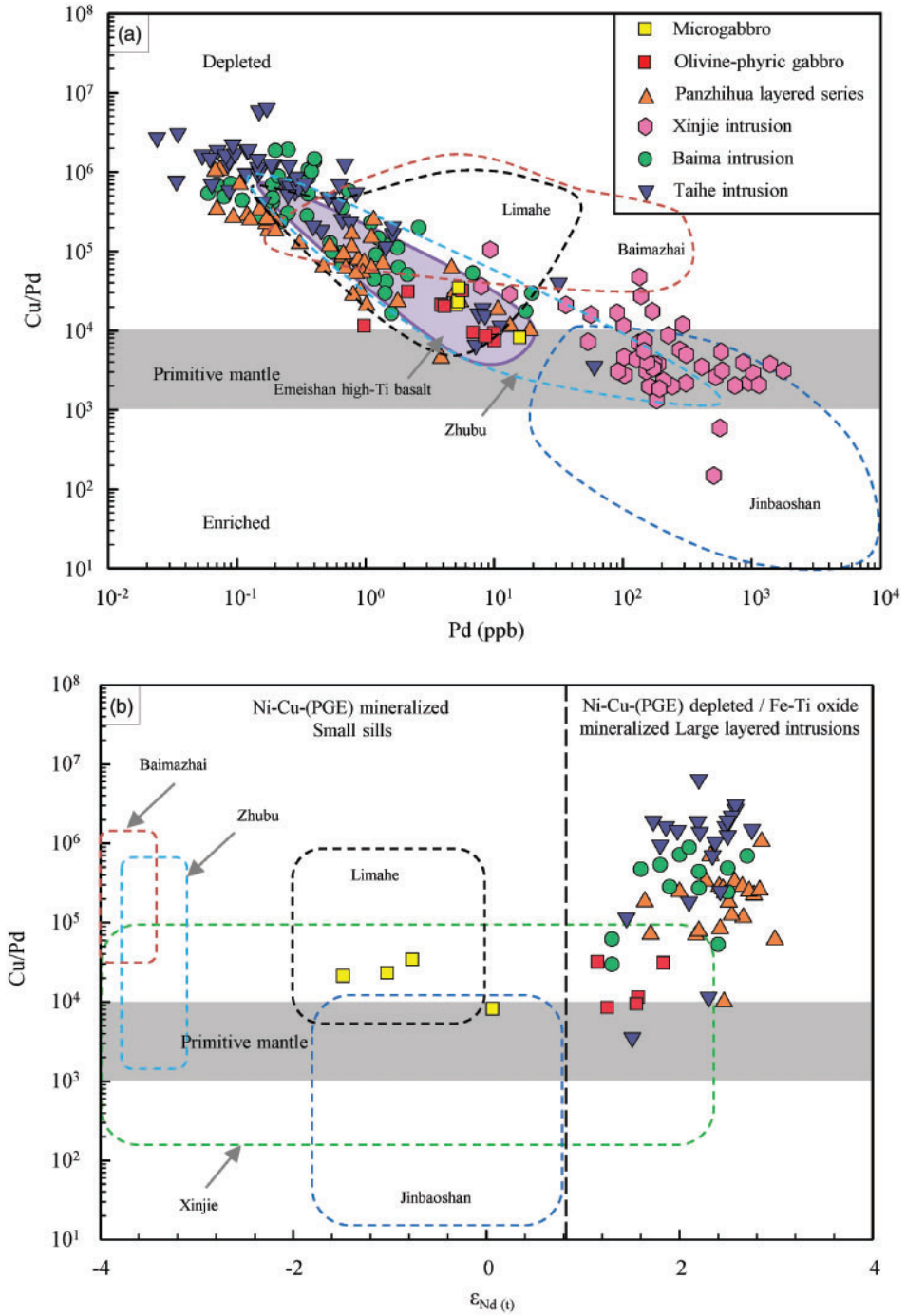

Fig. 10. Variation of Cu/Pd vs (a) Pd and (b) $\varepsilon_{Nd\ (t)}$ in the marginal rocks of the Panzhihua intrusion and the layered series of Fe–Ti oxide mineralized mafic–ultramafic intrusions in the Pan–Xi area. The compositions of Ni–Cu–(PGE) mineralized small sills are shown in the diagrams for comparison with the Fe–Ti oxide mineralized large layered intrusions. The data for Emeishan basalts are from GEOROC: (http://georoc.mpch-mainz.gwdg.de/georoc). Data sources for the mafic–ultramafic intrusions are from: Zhong *et al.* (2004); Wang *et al.* (2006); Tao *et al.* (2007, 2008); Zhou *et al.* (2008); Howarth & Prevec (2013); Tang *et al.* (2013); Zhang *et al.* (2013); Shellnutt *et al.* (2015); She *et al.* (2014, 2017).

clinopyroxene, plagioclase and Fe–Ti oxide from the Panzhihua, Baima and Taihe intrusions. The estimated $\delta^{18}O$ values ($\delta^{18}O$ =5·7–6·1‰) for the parental magmas of these intrusions are similar to mantle-derived magma and thus contamination by carbonates is negligible for these intrusions (Yu *et al.*, 2015). Moreover, the carbonate wall rocks have similar Nd isotopic compositions, but low Nd (≤0·27 ppm) contents, to those of the isotopically enriched microgabbros (Ganino *et al.*, 2008; Fig. 11). This suggests that the enriched Nd isotope compositions of these rocks cannot be attributed to wall rock contamination, but by assimilation of crustal

Table 3: Sr and Nd isotopic data for the Marginal Zone of the Panzhihua intrusion

Sample	Rock type	Rb (ppm)	Sr (ppm)	$^{87}Rb/^{86}Sr$	$^{87}Sr/^{86}Sr$	$\pm2\sigma$	$(^{87}Sr/^{86}Sr)_i$	Sm (ppm)	Nd (ppm)	$^{147}Sm/^{144}Nd$	$^{143}Nd/^{144}Nd$	$\pm2\sigma$	ε_{Nd} (t)
PZH1305	GB	13·6	204	0·192667	0·705219	9	0·704509	6·90	33·10	0·126014	0·512521	10	0·06
PZH1307	GB	3·96	591	0·019364	0·705435	10	0·705363	6·88	30·60	0·135914	0·512458	10	−1·49
PZH1309	GB	0·93	559	0·004782	0·705401	17	0·705383	7·17	32·90	0·131741	0·512475	11	−1·03
PZH1310	GB	0·75	669	0·003218	0·705341	11	0·705330	7·57	35·30	0·129634	0·512485	7	−0·77
PZH1301	OGB	15·60	361	0·124886	0·704753	12	0·704293	4·03	17·40	0·140008	0·512756	7	4·18
PZH1302	OGB	14·20	382	0·107429	0·705097	12	0·704701	4·25	17·90	0·143527	0·512756	8	4·06
PZH1303	OGB	8·41	188	0·129281	0·705344	14	0·704867	2·80	11·50	0·147183	0·512648	8	1·83
PZH1304	OGB	17·3	118	0·423703	0·706195	14	0·704634	2·20	8·77	0·151642	0·512642	7	1·57
PZH1406	OGB	43·5	215	0·584721	0·707050	9	0·704895	3·33	13·50	0·149110	0·512637	9	1·55
PZH1408	OGB	49·5	414	0·345543	0·706215	9	0·704941	4·98	21·90	0·137462	0·512655	10	2·30
PZH1409	OGB	10·9	438	0·071920	0·705508	14	0·705243	4·96	24·00	0·124930	0·512616	9	1·95
PZH1412	OGB	9·30	227	0·118401	0·705119	8	0·704683	3·75	17·60	0·128800	0·512582	10	1·15
PZH1413	OGB	9·87	240	0·118851	0·705049	10	0·704611	3·51	17·20	0·123360	0·512578	9	1·25
BCR-2					0·704990	6					0·512601	5	
BCR-2 recommend					0·705000						0·512636		

All the initial isotopic ratios were calculated to 259 Ma. ε_{Nd} values were calculated using $(^{147}Sm/^{144}Nd)_{CHUR(0)}=0·1967$ and $(^{143}Nd/^{144}Nd)_{CHUR(0)}=0·512638$.

materials at depth prior to injection into the Panzhihua magma chamber (Howarth & Prevec, 2013). Thus, the marginal rocks of the Panzhihua intrusion show relatively constant and low initial $^{87}Sr/^{86}Sr$ ratios (0·7043 to 0·7054), but highly variable Nd isotopic compositions (−1·49 to +4·18, Fig. 11), consistent with the interpretation that the magmas were contaminated by variable amounts of lower crustal materials and not by the adjacent country rocks. In contrast, the unique elevated initial ($^{87}Sr/^{86}Sr$) ratios of Ni–Cu-PGE mineralized intrusions such as the Limahe, Jinbaoshan and Zhubu intrusions in the ELIP (Zhou *et al.* 2008; Tao *et al.*, 2008) (Fig. 11) have been interpreted to be caused by variable contamination with mid/upper crustal materials. In this study, the results of mixing calculations imply that the marginal zone of the Panzhihua intrusion experienced <8 % contamination with lower-crustal materials (Fig. 11). A pulse of isotopically heterogeneous magma would homogenize during ascent from a staging magma chamber. The heterogeneous Sr–Nd isotopic compositions of the chilled marginal rocks of the Panzhihua intrusion indicate they were formed by multiple pulses of magmas in an open system. Variation of Sr–Nd isotopic compositions between each pulse of magma could be due to mixing between the contaminated residual magma and replenishing magma in a staging magma chamber.

Parental magma compositions and comparison with the coeval Emeishan basalts

The composition of the parental magmas of the Panzhihua deposit remains controversial. Previous research has used four main approaches to constrain the composition: (1) bulk mass summation; (2) estimation using gabbroic samples; (3) estimation using ultramafic dikes; and (4) estimation using coeval Emeishan flood basalts and associated melt inclusions. These different methods have yielded various parental magma compositions for the Panzhihua intrusion that are summarized in Table 4. Zhou *et al.* (2005) calculated the bulk composition of the intrusion by taking weighted mean compositions for each zone, yielding an estimated parental composition that is enriched in Fe and Ti. Zhang *et al.* (2009) suggested that the parental magma composition is close to gabbroic (PZH-1) and contained ∼12 wt % MgO and ∼17 wt % Fe_2O_3. In comparison, Hou *et al.* (2012) proposed an Fe-poor and Mg-rich liquid composition that is in equilibrium with olivine ($Fo_{90·4}$) based on ultramafic dikes that were intruded into the intrusion. The composition of the coeval Emeishan high-Ti basalts has also been suggested as a parental magma composition for the intrusions. The presence of significant amounts of Fe–Ti oxide mineralization within the mafic–ultramafic intrusions has led previous researchers to suggest that the parental magma was enriched in FeO and TiO_2, favoring the choice of the most Ti-rich basaltic magma to model petrological processes. Pang *et al.* (2008*a*) used an

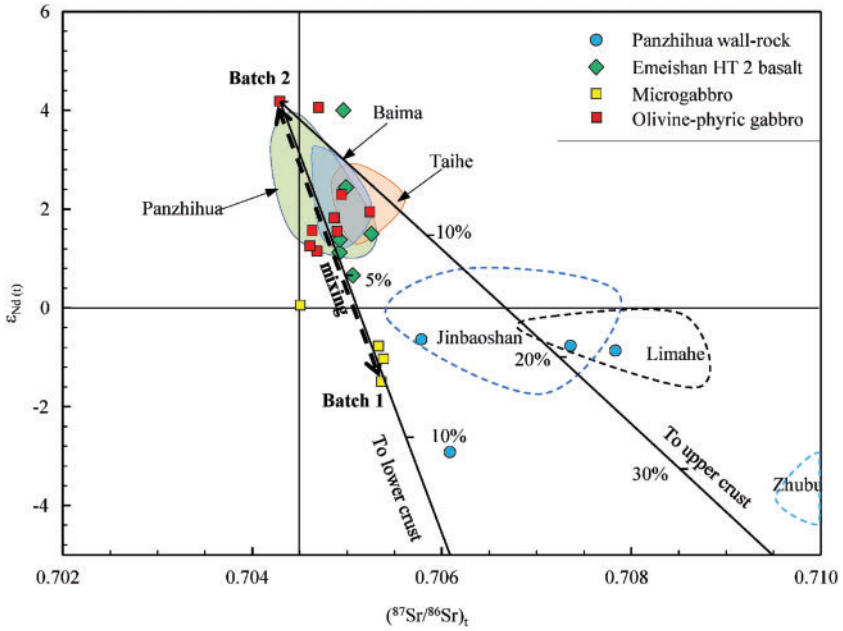

Fig. 11. Variation of $\varepsilon_{Nd\ (t)}$ vs $^{87}Sr/^{86}Sr_{(t)}$ for the marginal rocks of the Panzhihua intrusion and the layered series of Fe–Ti oxide mineralized mafic–ultramafic intrusions in the Pan–Xi area. The composition of Ni–Cu–(PGE) mineralized small sills are shown in the diagrams for comparison with the Fe–Ti oxide mineralized large layered intrusions. The parameters of Nd (ppm), $\varepsilon_{Nd\ (t)}$, Sr (ppm) and $^{87}Sr/^{86}Sr_{(t)}$ used in the mixing calculation are 18, 4·18, 180 and 0·704, respectively, based on Emeishan picrites, for the mantle-derived magma; 30·7, -38·5, 304, 0·713 and 26·6, -15, 273, 0·715 for the Yangtze lower and upper crust (Chen & Jahn, 1998; Gao *et al.*, 1998, 1999; Ma *et al.*, 2000). Data sources for the mafic–ultramafic the intrusions are: Zhong *et al.* (2004); Wang *et al.* (2006); Tao *et al.* (2007, 2008); Zhou *et al.* (2008); Howarth & Prevec (2013); Song *et al.* (2013); Tang *et al.* (2013); Zhang *et al.* (2013); She *et al.* (2014).

Emeishan basalt containing elevated concentrations of TiO_2 (4·85 wt %) to model the crystallization of Fe–Ti oxides within the Panzhihua deposit. A similarly high-Ti parental magma (TiO_2 = 4·9 wt %) derived from the composition of olivine-hosted melt inclusions within the Emeishan picrites was suggested by Song *et al.* (2013). In contrast, Ganino *et al.* (2008) used a basalt containing much lower concentrations of TiO_2 (TiO_2 = 2·6 wt %) in their petrological modeling. However, bulk mass summations are strongly dependent on correctly assuming volumes and compositions. The PZH-1 gabbro contains significantly lower SiO_2 (39 wt %) and incompatible trace element contents than the Emeishan basaltic magmas, indicating that these gabbros record crystal accumulation rather just the solidification of a melt. In addition, the liquid compositions derived from the ultramafic dikes are too MgO-rich to have directly generated the Panzhihua intrusion. Finally, the coeval high-Ti basalts have highly variable major element compositions (Xu *et al.*, 2001; Xiao *et al.*, 2004; Zhang *et al.*, 2006). For example, the TiO_2 contents of the high-Ti basalts vary between 2·5 and 5·2 wt % (Fig. 6a), meaning that it is unclear which of these basalts is representative of the composition of the Panzhihua parent magma.

The composition of magma parental to the olivine–phyric gabbros has been estimated using the method of Chai & Naldrett (1992). The line C to D in Fig. 6b represents the liquid compositions in equilibrium with the most primitive olivine (Fo_{83}) using the Mg–Fe olivine-liquid partition coefficient of 0·34 from Matzen *et al.* (2011). The FeO/FeO^{total} of the magma was adjusted for the FMQ + 1 buffer using the MELTS program of Ghiorso & Sack (1995). The estimated parental magma (point A) contains 8·2 wt % MgO, 13·.1 wt % FeO^{total} and 2·75 wt % TiO_2, similar to the compoition of the microgabbros and the neighboring Emeishan HT2 basalts (Fig. 6b). Small degrees of contamination by the lower crust of the Yangtze craton (εNd (t)=−38; Gao *et al.*, 1999; Ma *et al.*, 2000) would easily change the Nd isotopic composition of the mantle-derived magma without significantly changing its major element composition. Thus, each pulse of magma may have similar major element compositions, but slightly different isotopic compositions.

Fine-grained rocks within the marginal zones and associated flanking sills of mafic–ultramafic intrusions have long been considered to be representative of the parental magma composition of the intrusion (Wager, 1960). The best-known example of this is the Bushveld Complex, where different sections of marginal zone rocks (e.g. B-1, B-2 and B-3) reflect the parental magma compositions of different zones of the complex (Cawthorn *et al.*, 1981; Sharpe, 1981; Cawthorn & Davies, 1983; Sharpe & Hulbert, 1985; Barnes *et al.*, 2010; Wilson, 2012, 2015; Maier *et al.*, 2016). A similar interpretation can be made for the Panzhihua intrusion because: (1) The microgabbros occur at the base of the Panzhihua intrusion and represent the first phase of magma emplacement; (2) they are texturally and

Table 4: Proposed magmas parental to the Panzhihua intrusion

	Zhou *et al.* 2005	Pang *et al.* (2008a)	Ganino *et al.* (2008)	Zhang *et al.* (2009)	Song *et al.* (2013)	Hou *et al.* 2012	This study
SiO_2	42·6	45·83	45·7	39·63	41·8	–	45·45
TiO_2	3·99	4·85	2·6	4·31	4·92	–	2·73
Al_2O_3	15·8	15·62	13·2	9·94	13·6	–	12·61
Fe_2O_3	15·6	13·59	13·2	17·12	16·45	10	13·47
MnO	–	0·23	0·2	0·24	0·16		0·22
MgO	5·99	7·18	8·1	11·63	8·23	16	8·46
CaO	11·9	7·52	9·9	12·67	10·4	–	12·01
Na_2O	2·45	3·26	2·5	1·51	2·74	–	2·77
K_2O	0·31	1·41	1·6	0·23	0·91	–	0·29
P_2O_5	0·69	0·51	0·3	0·27	0·69	–	0·29
Total	99·2	100	97·3	97·55	99·9	–	98·30

mineralogically similar to quenched basalts; and (3) they have major and trace element and isotopic compositions that are remarkably similar to those of neighboring Emeishan HT2 basaltic magmas. However, the chilled marginal rock of the Bushveld Complex has also been interpreted to represent a derivative magma that escaped from the layered suite (Mungall *et al.*, 2016). Moreover, the marginal microgabbros in some intrusions are not primitive enough to be parental to the main portion of the layered intrusion, such as the Stillwater Complex (Raedeke, 1979; Jenkins & Mungall, 2018). Thus, whether the microgabbro compositions could represent the parental magma of the Panzhihua intrusion needs further examination.

Bai *et al.* (2014) estimated the trace element composition of the magma parental to the lower ore-bearing zone at the base of the Panzhihua intrusion using the average composition of clinopyroxene and the Cpx/liquid partition coefficients of Hill *et al.* (2000). The amounts of trapped liquid in these ore-bearing zone are less than <5% and thus have negligible effect on the compositional variation of incompatible trace element in the cumulus clinopyroxene crystals (Bai *et al.*, 2014). As shown in Fig. 8, the REE contents and patterns of the microgabbros are remarkably similar to the estimated liquid composition parental to the Lower Zone. Ti is known to be the element most resistant to diffusion in clinopyroxene (Cherniak & Liang, 2012). Hence, clinopyroxene could preserve its Ti concentration during trapped liquid shift or sub-solidus re-equilibration. The average TiO_2 content of clinopyroxene from the Lower Zone is about 1·04 wt % (Pang *et al.*, 2009). Using a partition coefficient of 0·38 for TiO_2 between clinopyroxene and basaltic magma from Hart & Dunn (1993), the concentration of TiO_2 in the parental magmas for the lower zone of the Panzhihua intrusion is estimated to be 2·7 wt %. Such a value well agrees with the average TiO_2 content of the microgabbros from the marginal zone (2·73 wt %, Table 4). Here, we use MELTS modeling (Ghiorso & Sack, 1995; Gualda *et al.* 2012) to determine whether the average composition of the microgabbros from the Panzhihua chilled margin is similar to the composition of the parental magma of the intrusion. This

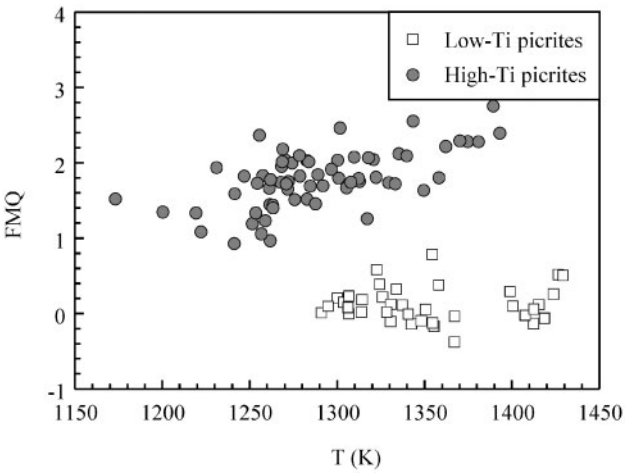

Fig. 12. Estimated oxidation state of the high-Ti and low-Ti basaltic magmas in the Emeishan LIP using the compositions of coexisting olivine and spinel from Emeishan picrites (Kamenetsky *et al.*, 2012). The fO_2 and temperature are calculated based on the methods of Ballhaus *et al.* (1990) and Ballhaus *et al.* (1991), respectively.

approach involves modelling the liquid line of descent for the mafic rocks within the intrusion and the composition of the phases in equilibrium with these liquids. The oxygen fugacity is fixed at FMQ + 1, close to the lower end of the oxygen fugacities calculated for the Emeishan high-Ti picrites (Fig. 12). The pressure is set at 1 kbar according to Song *et al.* (2013) and the bulk H_2O content is assumed to be 0·1 wt %. Pang *et al* (2008*a*) summarized the following crystallization order on the basis of the cumulus stratigraphy: clinopyroxene + plagioclase + titanomagnetite ± olivine → olivine + clinopyroxene + plagioclase + titanomagnetite + ilmenite→olivine + clinopyroxene + plagioclase + titanomagnetite + ilmenite + apatite. In this study, the first phase to crystallize from the melt was Cr-rich titanomagnetite, consistent with the observation of Pang *et al.* (2008*a*) that abundant Cr-rich titanomagnetite occurs as inclusions in relatively primitive olivine and clinopyroxene. Then titanomagnetite, clinopryoxene (Mg#81), plagioclase (An71) and olivine (Fo_{82}) almost

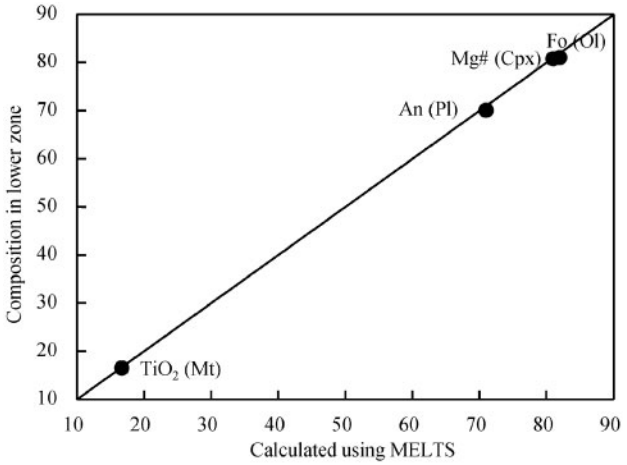

Fig. 13. Comparison of the calculated Fo content of olivine, Mg# of clinopyroxene, An content of plagioclase and TiO_2 content of titanomagnetite in equilibrium with the average composition of the microgabbros using MELTS (Ghiorso & Sack, 1995; Gualda *et al.* 2012) and the most primitive composition from the Lower Zone of the Panzhihua intrusion. The compositions of olivine, clinopyroxene, plagioclase and titanomagnetite are from Pang *et al.* (2008*b*, 2009).

contemporaneously crystallized from the magma over a short temperature interval (1199°C∼1167°C), consistent with the mineral associations (clinopyroxene + plagioclase +titanomagnetite ± olivine; Pang *et al.*, 2008*a*) in the Lower Zone. Moreover, the compositions of silicate minerals (olivine, clinopyroxene and plagioclase) calculated using MELTS are very close to the most primitive compositions (Fo_{81}, Mg#81 and An_{70}; Pang *et al.*, 2009) of those from the Lower Zone (Fig. 13). Experimental studies have indicated that the TiO_2 content of magnetite negatively correlates with the fO_2 of the magma in which it crystallized (Buddington & Lindsley, 1964; Hill & Roeder, 1974; Toplis & Carroll, 1995). The simulated and measured TiO_2 contents of titanomagnetite are in good agreement with each other (Fig. 13), suggesting that it is appropriate to use this fO_2 (FMQ + 1) in MELTS modeling. Ilmenite and apatite crystallized from the magma at a later stage (1097°C and 1043°C), corresponding to the observed mineral assemblages at the top of the MZa (olivine + clinopyroxene + plagioclase + titanomagnetite + ilmenite) and MZb (olivine + clinopyroxene + plagioclase + titanomagnetite + ilmenite + apatite), respectively (Pang *et al.*, 2009). In summary, our modeling results match the crystallization order and mineral compositions within the main body of the Panzhihua intrusion (Pang *et al.*, 2009). This, together with the consistent REE and TiO_2 contents between microgabbros and the estimated magma parental to the Lower Zone suggest that the average composition of the chilled microgabbros is similar to the parental magma for the Panzhihua intrusion.

Although the parental magma of the microgabbros was subjected to minor contamination by mafic lower crust as demonstrated above, the process could not significantly change the major composition of the magma, due to the low proportion (<8%) of the contaminant and small difference in composition between basaltic magma and mafic lower crust.

The data presented in this study indicate that the parental magma of the Panzhihua intrusion contained ∼8·46 wt % MgO, 13·47 wt % Fe_2O_3 and ∼2·73 wt % TiO_2. This concentration of TiO_2 is close to the lower end (2·5 wt %) of the TiO_2 contents of the high-Ti basalts within the ELIP. Our suggested TiO_2 content is obviously lower than the maximum concentrations (up to 5 wt %; Fig. 6a) of the high-Ti basalts of the ELIP, despite the fact that the latter was previously considered to represent the parental magma for the Panzhihua intrusion (Pang *et al.*, 2008*a*; Song *et al.*, 2013) and for other Fe–Ti oxide mineralized intrusions within the ELIP (e.g. the Hongge intrusion, Bai *et al.*, 2012*b*; Luan *et al.*, 2014; the Baima intrusion, Zhang *et al.*, 2012). Therefore, it is suggested that a TiO_2-rich parental magma is not necessary for the generation of the giant magmatic Fe–Ti oxide deposits within the ELIP. The relatively low TiO_2 contents of the Panzhihua parental magmas are consistent with the composition of the main oxide ores in the Lower Zone of the intrusion, which contain only rare ilmenite and are dominated by titanomagnetite (Pang *et al.*, 2008*a*, 2008*b*; Howarth *et al.*, 2013).

Sulfide saturation in the Panzhihua plumbing system

It is well known that magnetite-rich cumulates within layered mafic–ultramafic intrusions can be enriched in PGE, as exemplified by the Stella Intrusion in South Africa (Maier *et al.*, 2003), the Rio Jacaré intrusion in Brazil (Sa *et al.*, 2005), the Skaergaard Intrusion in Greenland (Nielsen *et al.*, 2015), the Rincón del Tigre Complex in Bolivia (Prendergast, 2000) and the Freetown Intrusion in Sierra Leone (Bowles *et al.*, 2013). The most recently identified examples of this style of mineralization include the Jameson Range layered intrusion in Australia (Karykowski *et al.*, 2017) and the Mesoarchean Nuasahi Massif in India (Prichard *et al.*, 2017). The only magnetite-rich cumulates that contain elevated concentrations of PGE (up to 1·2 ppm Pt and 1·8 ppm Pd) within the ELIP are located in the smaller Xinjie Fe–Ti oxide-bearing, mafic–ultramafic layered intrusion (Zhong *et al.*, 2011*b*). Most of the other larger Fe–Ti oxide mineralized mafic–ultramafic layered intrusions within the ELIP (e.g. the Panzhihua, Hongge, Baima and Taihe intrusions; Bai *et al.*, 2012*a*; Howarth & Prevec, 2013; Zhang *et al.*, 2013; Shellnutt *et al.*, 2015; She *et al.*, 2017) are depleted in PGE (Fig. 10). For example, the Panzhihua intrusion has very low total PGE contents (≪5ppb) and high Cu/Pd ratios (24 000–250 000) (Howarth & Prevec, 2013). Previous studies have suggested that the coeval high-Ti and low-Ti basalts were generated by different degrees of (high-Ti

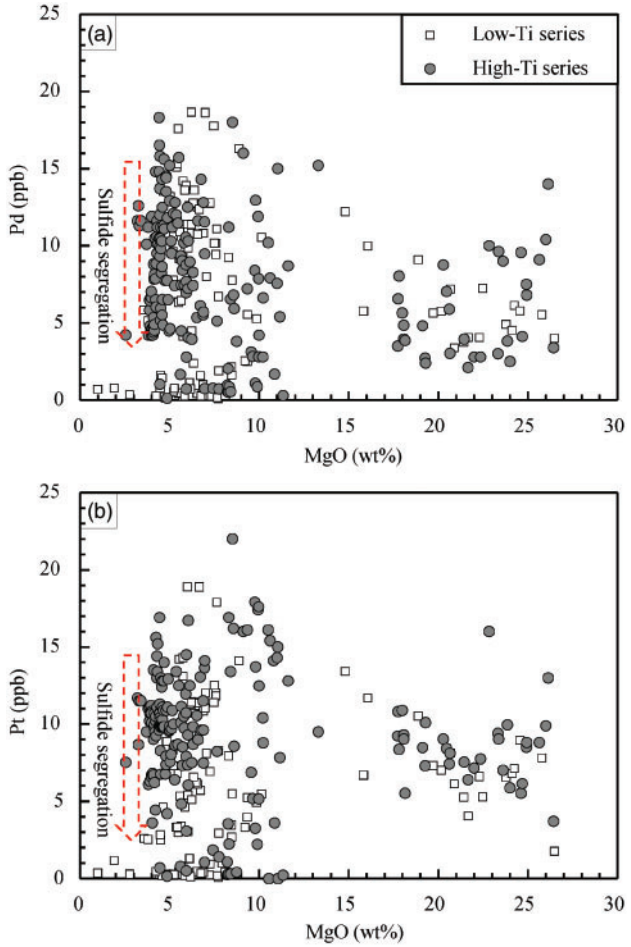

Fig. 14. Variation of whole-rock MgO vs (a) Pd and (b) Pt for the Emeishan high-Ti and low-Ti basalts and picrites. Data sources are from GEOROC: (http://georoc.mpch-mainz.gwdg.de/georoc).

series < 8% and low-Ti series > 20%) partial melting of different mantle sources (Xu *et al.*, 2001; Xiao *et al.*, 2004; Zhang *et al.*, 2006; Wang *et al.*, 2007). A degree of partial melting of <8% is insufficient for the high-Ti melt to dissolve the entire sulfide in the mantle source at lower fO_2 (Keays, 1995; Yao *et al.*, 2018). It has been shown that the parental magmas of these layered intrusions are similar to the high-Ti series. As a result, PGE depletion in the Panzhihua and other layered intrusions could be due to sulfide retainment in the mantle source at low degrees of partial melting. If this is the case, all the Emeishan high-Ti series should be depleted in PGE. However, as shown in Fig. 14, the published Pt and Pd contents of the high-Ti and low-Ti series exhibit no differences. Particularly, more than half of the high-Ti samples have undepleted PGE contents (i.e. Pt+Pd > 20ppb), suggesting almost all the sulfides had been removed from the mantle source. Sisson (2003) and Mungall *et al.* (2006) indicated that small-degree melts with elevated PGE contents were generated at moderately high oxygen fugacity. As shown in Fig. 12, the fO_2 of the high-Ti series ranges from FMQ + 1 to FMQ + 2·5, while that of low-Ti series was around FMQ.

Experimental studies have shown that the S^{6+}/S^{2-} ratios and S contents at sulfide saturation in basalts increase with elevated fO_2 over the interval of FMQ∼FMQ + 2 (Jugo, 2009; Jugo *et al.*, 2010). The estimated S content at sulfide saturation ranges from 1500 ppm at FMQ + 0·5 to 4500 ppm at FMQ + 1·7 (Jugo, 2009). Thus, a relatively low degree of partial melting (<8%) is sufficient for the high-Ti melt to dissolve the entire sulfide in the mantle source at FMQ + 1 to FMQ + 2·5. This in turn means that the PGE-depleted nature of these intrusions most likely relates to the early removal of sulfides from the primary magmas at depth (Bai *et al.*, 2012*a*; Howarth & Prevec, 2013; Zhang *et al.*, 2013; Shellnutt *et al.*, 2015; She *et al.*, 2017). Sulfide inclusions within the olivine phenocrysts (Fig. 3f) are consistent with the interpretation of early sulfide removal at depth. The relatively low Cu contents of the chilled marginal samples, as analysed during this study, relative to melt inclusion Cu concentrations (Fig. 7d) and the elevated Cu/Pd ratios of these samples ($0{\cdot}75 \times 10^4$–$3{\cdot}44 \times 10^4$, Fig. 10) relative to the mantle values (10^3–10^4 range with median values of 5488, Barnes *et al.*, 2015), also provide evidence of early sulfide removal. In addition, the marginal rocks contain much higher quantities of S (up to 1·48 wt %; Table 1) than the maximum S content at sulfide solubility of these magmas. In other words, the PGE concentrations of the chilled marginal samples were controlled by sulfides accumulated from a previously PGE-depleted magma.

Sulfur is incompatible in silicates and oxides and S concentrations will increase in residual melts during fractional crystallization. This led Zhang *et al.* (2013) and She *et al.* (2017) to suggest that the PGE-depleted parental magmas of the ELIP intrusions recorded early stage sulfide saturation as a result of the extensive fractionation of chromite, olivine and clinopyroxene at depth. Sulfide saturation is generally not achieved until 45%–50% of a batch of magma has crystallized (Naldrett, 2010). Combining MELTS modeling with the equation outlined by Li & Ripley (2009) indicates that at least 42–59% fractional crystallization of a primary picritic magma is required to induce sulfide saturation if no external S is involved (Bai *et al.*, 2012*a*; Zhang *et al.*, 2013; She *et al.*, 2017). This is consistent with the fact that the most evolved and PGE-undepleted Emeishan high-Ti basalts (Pt + Pd ≥ 20 ppb) have MgO contents as low as 3·2–4·5 wt % (Qi & Zhou, 2008; Song *et al.*, 2009; Fig. 14). However, modelling by Howarth & Prevec (2013) has shown that the parental magma of the Panzhihua intrusion experienced approximately 25% fractional crystallization from a picritic magma. Thus, Howarth & Prevec (2013) suggested that the early stage sulfide saturation of the primary magma for these intrusions at depth was not triggered by fractional crystallization alone. The relatively high forsterite contents (up to $Fo_{77–88}$; Pang *et al.*, 2008*a*, 2016; Zhang *et al.*, 2012) of the olivines within other PGE-depleted intrusions also do not support a model where sulfide saturation was triggered by extensive fractionation.

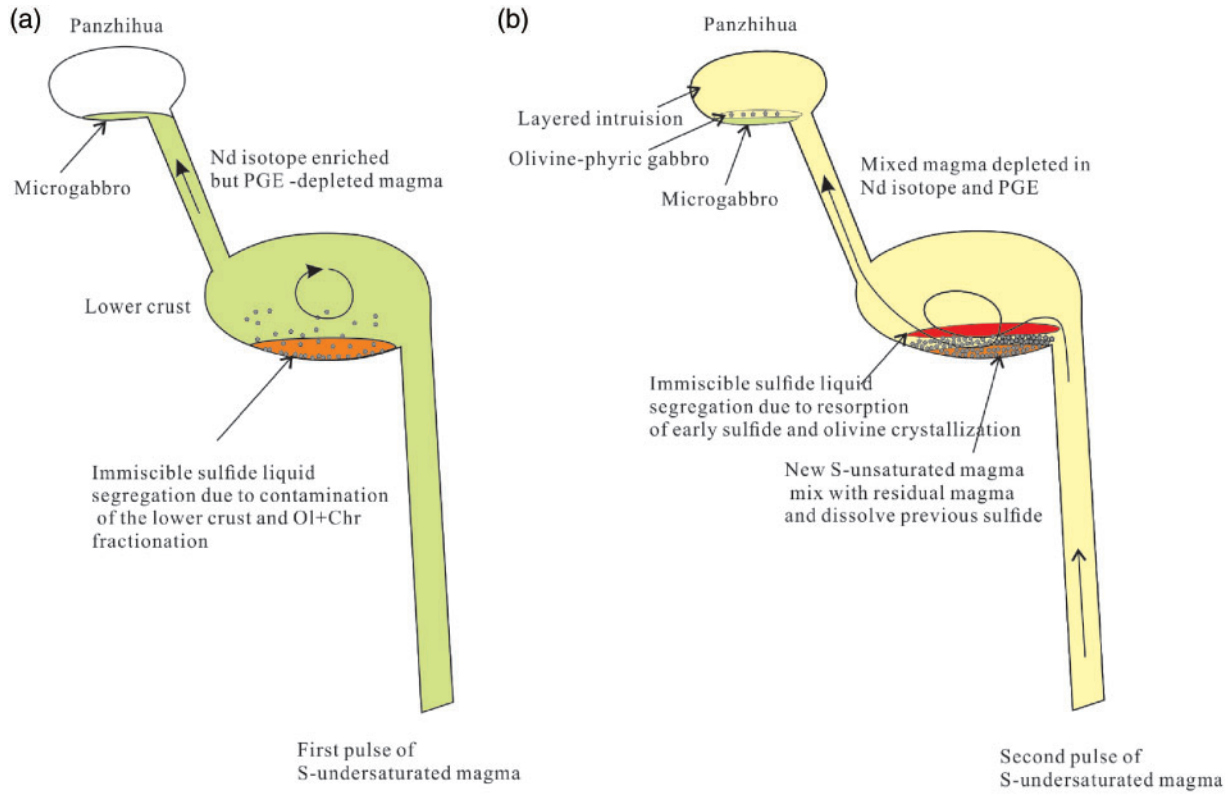

Fig. 15. A schematic model for the sulfur saturation process in the magma parental to the Fe–Ti oxide mineralized large layered intrusions.

The addition of external S via crustal contamination during fractional crystallization is thought to be a key process in the sulfide saturation of ELIP magmas (Wang & Zhou, 2006; Tao *et al.*, 2008; Song *et al.*, 2009; Bai *et al.*, 2012*a*; Howarth & Prevec, 2013; Shellnutt *et al.*, 2015). The enriched Nd isotopic compositions (Figs 10b and 11; -8·4 to +0·81; Wang *et al.*, 2006; Tao *et al.*, 2008; Zhou *et al.*, 2008; Tang *et al.*, 2013) and non-mantle $\delta^{34}S$ values (Limahe = 2·44 to 5·4, Tao *et al.*, 2008; Jinbaoshan = -23·0 to +18·5, Tao *et al.*, 2007) of typical magmatic Ni–Cu–PGE sulfide deposits within the small sills in the ELIP can be explained by the additional of external S via crustal contamination (Figs 10b and 11). However, the large PGE-depleted layered mafic–ultramafic intrusions, including the Panzhihua, Baima and Taihe intrusions, have Sr–Nd isotopic compositions that overlap with, or are even more depleted than, the PGE-undepleted picrites and the Xinjie intrusion (Figs 10b, 11), suggesting negligible crustal contamination in terms of the sulfide saturation of these magmas at depth. This inference is further supported by the mantle-like $\delta^{18}O$ (5·7– 6·1‰, Yu *et al.*, 2015) and $\delta^{34}S$ (-0·5–2·66‰, Pang, 2008; Zhang *et al.*, 2013) values of the parental magmas for these intrusions. These results, therefore, contradict the model that ascribes the early-stage sulfide saturation of the primary magma of these intrusions at depth to the addition of external S via crustal contamination. Consequently, the most reasonable explanation for this S-saturation event is the addition of S from magmatic rocks that had similar Sr–Nd–O–S isotopic compositions to the layered intrusions. The best candidate for this is the product of basaltic magmas that also formed part of the ELIP plumbing system. Here, we propose a new model for early-stage sulfide saturation at depth, as illustrated in Fig. 15 and summarized here. An early pulse of mantle-derived, S-undersaturated and Nd isotope depleted magma was injected into a staging magma chamber at a lower crustal level. The magma contains higher PGE contents because it was generated by lower degree of partial melting at relatively higher fO_2 (FMQ + 1 to FMQ + 2·5). Assimilation of the lower crustal materials plus extensive differentiation would have resulted in S saturation of the magma and the segregation of an immiscible sulfide liquid within the deep magma chamber (Howarth & Prevec, 2013; Fig. 15a). Part of the residual magma was emplaced into the shallow crust, generating a chilled microgabbro with an enriched in Nd isotope composition at the base of the Panzhihua intrusion. A new pulse of S-undersaturated and Nd isotope depleted magma ascending from the mantle was injected into the staging magma chamber, subsequently mixed with the residual S-saturated magma and progressively dissolved the previously existing sulfide liquid (Fig. 15b). The S content of this magma was strongly enhanced by the resorption of early-formed sulfides. Then the mixed magma reached S saturation after a short period of olivine crystallization. Sulfide

liquid segregation within the deep magma chamber, along with olivine crystallization, resulted in PGE, Ni and Cu depletion of the new pulse of magma. Finally, the magma with some earlier-formed olivines entered the Panzhihua magma chamber, to form the more Nd isotope depleted olivine–phyric gabbros overlying the microgabbros and ultramafic to mafic sills (picritic dykes) that penetrated into the country rocks. The Panzhihua layered intrusion formed by later influxes of the mixed magma, as shown by the mixed trend of Sr–Nd isotopic compositions (Fig. 11). This means that the deep-seated mafic–ultramafic intrusion beneath the PGE-depleted ELIP intrusions represents an important exploration target for Cu–Ni–PGE deposits within the ELIP. The grade and tonnage of these deep-seated potential Cu–Ni–PGE deposits could be considerable, as the huge volume of magma that formed the shallow Fe–Ti oxide mineralized intrusions is depleted in PGE. However, the depths of these deep-seated staging magma chambers within the ELIP remain unclear. Pang *et al.* (2008*b*) suggested that the parental magmas of the Panzhihua intrusion may have formed by differentiation of mantle-derived picritic melts at a pressure of ~10 kbar, probably close to the base of the crust. Wang *et al.* (2014) and Tao *et al.* (2015) estimated a similar pressure for the high-Ti ultramafic rocks and picrites. In this study, the Sr–Nd isotopic compositions of the microgabbros indicate that the staging magma chamber was located in the lower crust, consistent with previous suggestions. Comprehensive geophysical research has identified a distinct region at the base of the crust within the Inner Zone of the ELIP (i.e. the Pan–Xi area), marked by high density, high P-wave velocities and high Vp/Vs ratios (Chen *et al.*, 2015). This section is thought to be a mafic–ultramafic layer generated by magmatic underplating associated with the Emeishan mantle plume (Xu & He, 2007; Chen *et al.*, 2015). This large mafic–ultramafic layer at the base of the crust may represent the deep-seated magma chamber where sulfide saturation occurred. If this is the case, then it is unlikely that the ELIP contains voluminous economic magmatic Cu–Ni–PGE sulfide mineralization. A recent study suggested that the late Permian bimodal volcanic rocks in the Northern Qiangtang terrane were generated from interaction between the Emeishan plume and the Paleo-Tethyan subduction system (Wang *et al.*, 2018). If plume-subduction interaction also occurred in the Pan–Xi area, the remelting of these mafic cumulates, rich in sulfides and Cu–Au–PGE, at the base of the crust could lead to the genesis of porphyry Cu–Au deposits if this remelting occurred under certain conditions (Lee *et al.*, 2012; Chiaradia, 2014; Jenner, 2017).

Implications for the formation of Fe–Ti oxide deposits

The processes involved in the formation of the Fe–Ti oxide deposit within the Panzhihua intrusion remain unclear. Three main models have been proposed for the generation of this mineralization: (1) the crystallization of Fe–Ti oxides within a deep magma chamber before these oxides were transported to their current position as crystal-rich slurries (Howarth *et al.*, 2013); (2) formation from an immiscible Fe-rich liquid (Zhou *et al.*, 2005; Xing *et al.*, 2014); and (3) early crystallization from a basaltic parental magma (Ganino *et al.*, 2008; Pang *et al.*, 2008*a*, 2008*b*, 2009; Song *et al.*, 2013).

Howarth *et al.* (2013) suggested that the main Fe–Ti oxide ore layers within the Panzhihua intrusion did not form *in situ* but instead accumulated from crystal-rich titanomagnetite slurries generated in a deeper magma chamber. This is analogous to the model suggested for the generation of the chromitite layers within the Bushveld Complex (Eales, 2000; Mondal & Mathez, 2007; Voordouw *et al.*, 2009; Eales & Costin, 2012). More than 30 Fe–Ti oxide-mineralized mafic–ultramafic intrusions are present within this area (Song *et al.*, 2013). Since titanomagnetite can be transported to shallow magma chambers to form Fe–Ti oxide deposits, it should also be carried to the surface to form magnetite-phyric basalts. However, previous studies have indicated that the phenocrysts in the Emeishan basalts and picrites are olivine, augite and plagioclase (Xu *et al.*, 2001; Xiao *et al.*, 2004; Zhang *et al.*, 2006; Kamenetsky *et al.*, 2012). Coarse-grained Fe–Ti oxide phenocrysts are not observed in the Emeishan LIP. The composition of titanomagnetite would vary randomly within the ore layers if they were accumulated from crystal-rich titanomagnetite slurries. However, the upward decrease in magnetite Cr contents and the positive correlation between the Cr contents of magnetite and associated clinopyroxene within each cycle of the Panzhihua and Hongge intrusions (Bai *et al.*, 2012*b*; Chen *et al.*, 2017) do not favor this model and suggest that these magnetites crystallized at the same time as the clinopyroxene within the magma chambers that are represented by these two intrusions. Thus, it is preferable to suggest that this model is less favored than alternatives which allow for *in situ* titanomagnetite precipitation. Based on the cumulus nature of the HFSE anomalies, Howarth & Prevec (2013) also suggested that the titanomagnetite within the ore layer crystallized within the main Panzhihua chamber.

Zhou *et al.* (2005) and Xing *et al.* (2014) described a ferrobasaltic parental magma that was separated into a silicate magma and an Fe–Ti-rich melt within the magma chamber occupied by the intrusion, where the immiscible Fe–Ti-rich melt migrates toward the base of the chamber to form the main Fe–Ti oxide ores. The onset of silicate liquid immiscibility generally occurs during the final stages of the evolution of mafic magmas, yielding an Fe–Ti–P-rich melt that can produce ilmenite–magnetite–apatite-rich rocks associated with evolved plagioclase and low-Mg# ferromagnesian silicates (Philpotts & Doyle, 1983; Charlier & Grove, 2012; Charlier *et al.*, 2015). However, the massive Fe–Ti oxide ore layers within the Panzhihua intrusion are dominated by titanomagnetite and contain only rare ilmenite and

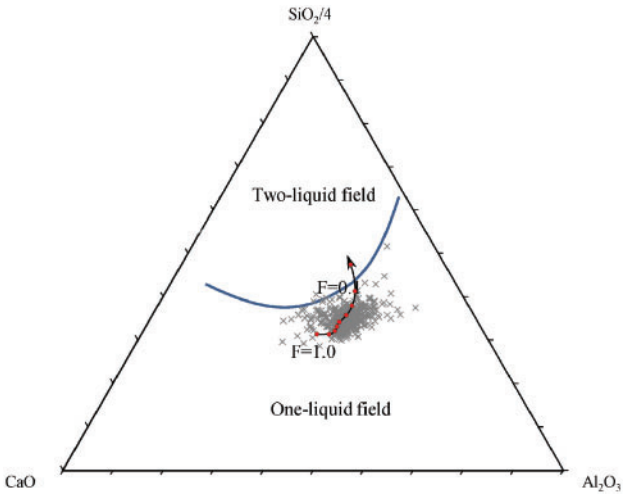

Fig. 16. Panzhihua parental magma liquid line of descent and the composition of Emeishan high-Ti basalts (MgO = 2∼12 wt %) in the ternary diagram SiO_2/4–CaO–Al_2O_3. One-liquid field, two-liquid fields and the position of the binodal are from Charlier & Grove (2012). F: Fraction of residual liquid. The data for Emeishan basalts are from GEOROC: (http://georoc.mpch-mainz.gwdg.de/georoc).

apatite. Experiments on immiscible melts in natural immiscible globules enabled Charlier & Grove (2012) and Charlier *et al.* (2013) to construct ternary diagrams that define the location of one- and two-liquid fields for these systems. The MELTS-based liquid lines of descent for the parental magmas of the Panzhihua intrusion are plotted in the ternary diagram in Fig. 16. The compositions of the parent magma is far away from the two-liquid field, thus it could cross the binodal curve and enter the two-liquid immiscibility field only after extensive fractional crystallization (e.g. >70%). This indicates that liquid immiscibility played little role in the generation of the Fe–Ti oxide ores within the intrusion. In fact, the main Fe–Ti oxide ores coexist with primitive silicate minerals within the lower part of the intrusion, whereas apatite coexists with evolved silicate minerals within overlying layers. Thus, liquid immiscibility played a role in the formation of the most evolved apatite-bearing gabbros at the top of the MZb, if this liquid immiscibility process actually happened during crystallization. The compositions of the Emeishan high-Ti basalts are also projected onto this ternary diagram. The MgO contents of the basalts range between 12 wt % and 2 wt %, representing the products of different degrees of fractional crystallization. The result shows that almost all the compositions of the Emeishan high-Ti basalts plot within the one-liquid stability field and far away from the binodal curve. This suggests that the high-Ti series magma did not enter the two-liquid immiscibility field until the final stages of the magma evolution. Howarth & Prevec (2013) showed that the main ore layers exhibit positive Zr–Hf and Nb–Ta anomalies. The compatible behavior of HFSE indicates cumulus ore formation processes rather than formation from an immiscible Fe-liquid (Howarth & Prevec, 2013). Most olivines in the Panzhihua layered series have Ni contents <250 ppm (Pang *et al.*, 2009; Song *et al.*, 2013; Fig. 5b), much lower than those in the Marginal Zone. Such extremely low Ni contents of olivine in the layered series cumulates is unlikely due to sulfide removal. Ni is more compatible in magnetite (D_{Ni}=31–65, Nielsen *et al.*, 1994) than in olivine. Hence, the low Ni content in olivine could be caused by competition for Ni between olivine and magnetite during cotectic crystallization. This in turn supports the idea that magnetite crystallized from the magma at an early stage of differentiation together with olivine.

An unusual feature of these Fe–Ti oxide mineralized intrusions is that the silicate minerals (olivine, clinopyroxene and plagioclase) in these intrusions are significantly more primitive than those in other magmatic Fe–Ti oxide deposits elsewhere at the onset of Fe–Ti oxide saturation (Bai *et al.*, 2012*b*; Pang *et al.*, 2009). Tang *et al.* (2017) proposed that contamination by dolomite wall rocks introduced MgO into the basaltic magma, which in turn produced the association of Mg-rich olivine with magnetite. The $\delta^{18}O$ values of the dolomite footwall rocks (24·6–28·6‰; Ganino *et al.*, 2013) are much higher than those of mantle-derived magmas (5·7‰; Eiler, 2001). Thus, a small amount of dolomite contamination would significantly elevate the $\delta^{18}O$ values of the basaltic parental magma. Yu *et al.* (2015) determined the oxygen isotopic compositions of clinopyroxene, plagioclase and Fe–Ti oxides from the Panzhihua, Baima and Taihe intrusions. The estimated $\delta^{18}O$ values ($\delta^{18}O$ =5·7–6·1‰) for the parental magmas of these intrusions are similar to those of mantle-derived magma (5·7‰; Eiler, 2001) and thus contamination by dolomite is negligible for these intrusions (Yu *et al.*, 2015). On the other hand, if considerable MgO was added to the parental magma by dolomite contamination, the crystallized olivine could obviously deviate from the NiO–Fo and MnO–Fo array defined by the picrites, because Ni and Mn were not added to the magma with MgO synchronously. However, clear deviation has not been observed in these layered intrusions (Fig. 5a, b). Some researchers have suggested that the Fe–Ti oxides directly crystallized from a basaltic parental magma at an early stage of differentiation and then formed the ore layers by gravitational settling (Ganino *et al.*, 2008; Pang *et al.*, 2008*a*, 2008*b*, 2009; Song *et al.*, 2013). However, the cause of early saturation of Fe–Ti oxides in these intrusions remains debated (Ganino et al., 2008; Zhang *et al.*, 2009; Song *et al.*, 2013; Luan *et al.*, 2014; She *et al.*, 2014).

Several studies (Zhang *et al.* 2009; Song *et al.*, 2013; She *et al.*, 2014) have proposed that the early crystallization of Fe–Ti oxides was controlled mainly by high Fe and Ti concentrations in the parental magmas. Such an Fe–Ti-enriched magma has been attributed to the characteristics of its mantle source (Zhang *et al.*, 2009) or produced by fractionation of picritic magma at depth (Song *et al.*, 2013). However, the predicted parental magma of the Panzhihua intrusion only contains 13·5 wt

% FeO_T and 2·7 wt % TiO_2 (Table 4) and thus does not support these hypotheses. Oxygen fugacity is known to have a significant influence on the saturation of Fe–Ti oxides in mafic magmas (Toplis & Carroll, 1995). The low V concentrations in the Fe–Ti oxides, which are sensitive to redox, indicate that the relatively early saturation of Fe–Ti oxides in the Panzhihua and Hongge magmatic systems was caused by higher oxidation states (Ganino *et al.*, 2008; Pang *et al.*, 2008*a*; Bai *et al.*, 2012*b*). The MELTS modeling undertaken at an fO_2 of FMQ + 1 during this study clearly demonstrates that Fe–Ti oxides, as well as other minerals, crystallized from the parental magma composition determined in this study, with the predicted mineral compositions corresponding to the compositions of minerals within the main body of the Panzhihua intrusion. Our results further support the interpretation of early crystallization from a basaltic parental magma. Ganino *et al.* (2008) suggested that oxidation of the basaltic parental magma by release of CO_2-rich fluids from the dolomite country rocks has played a major role in the early saturation of Fe–Ti oxides. However, based on the oxygen isotopic compositions of clinopyroxenes in these mineralized intrusions, Yu *et al.* (2015) argued that such a process is not sufficient to increase the oxidation state of the magma. We calculated the fO_2 of the Emeishan basaltic magma using the composition of coexisting olivine and spinel in picrites that are not contact with the dolomite wall rocks (Kamenetsky *et al.*, 2012). The results show that the high-Ti series (FMQ + 1∼FMQ + 2·5) are more oxidized than the low-Ti series (FMQ) (Fig. 12). Recent studies have confirmed that mantle plume-derived magmas have a relatively oxidized nature at around QFM + 1 (e.g. Moussallam *et al.*, 2016; Brounce *et al.*, 2017; Hartley *et al.*, 2017). Thus, relatively, the high oxygen fugacity of the high-Ti parental magmas in the ELIP might be inherited from an oxidized mantle source.

CONCLUSIONS

The chilled marginal rocks of the Panzhihua intrusion consist of microgabbros and olivine–phyric gabbros that are present at the base of the intrusion and represent the first stage of magma emplacement. This zone is texturally and mineralogically similar to quenched basaltic magma and as such represents the chilled marginal rocks of the Panzhihua intrusion. The olivine–phyric gabbros consist of variable proportions (20%–60%) of coarse-grained olivine within a fine-grained matrix. The microgabbros are compositionally similar to the neighboring Emeishan HT2 basalts in terms of their major and trace element contents. Combining these characteristics with the fact that the microgabbros are mineralogically and compositionally consistent with the overlying layered series of the intrusion and the results of MELTS modeling of these microgabbros, suggests that the average compositions of the fine-grained microgabbros within the Marginal Zone could indeed record the composition of the parental magma of the Panzhihua intrusion. The relatively low TiO_2 content (∼2·73 wt %) of the parental magma relative to the maximum concentration of TiO_2 (up to 5 wt %) within the high-Ti basalts in the ELIP indicates that the formation of giant magmatic Fe–Ti oxide deposits does not require extremely high TiO_2 contents, as was proposed previously.

The heterogeneous isotopic compositions of the chilled margin rocks indicate they were formed by multiple pulses of magma in an open system. Relatively constant and low initial $^{87}Sr/^{86}Sr$ ratios, but highly variable Nd isotopic compositions, are consistent with the interpretation that the magmas were contaminated by variable amounts (<8%) of lower crustal materials.

Sulfide inclusions within olivine, together with the elevated Cu/Pd ratios and relatively low Cu contents of the microgabbros, suggest that early sulfide removal took place in a deep-seated magma chamber. The relatively primitive compositions of the minerals within the Fe–Ti mineralized intrusions of the ELIP suggest that sulfide saturation was not triggered by extensive fractionation. However, the depleted Sr–Nd isotopic compositions and the mantle-like $\delta^{18}O$ and $\delta^{34}S$ values of these intrusions do not support a model in which S saturation was induced by crustal contamination. We propose that crustal contamination plus fractionation within an early pulse of mantle-derived, S-undersaturated magma in a deep-seated magma chamber in the lower crust caused S saturation and the segregation of an immiscible sulfide liquid. Such a PGE-depleted and Nd isotope enriched magma was subsequently emplaced into the shallow crust to form the chilled microgabbros. A new pulse of S-undersaturated magma mixed with the residual magma and dissolved earlier-formed sulfide liquid, causing S saturation of the new pulse of magma during the early stages of differentiation. The resulting PGE-depleted magma was emplaced into the shallow crustal chamber, along with olivine captured from the mush, forming the olivine–phyric gabbros and overlying layered intrusion. Such processes would not change the mantle-like Sr–Nd–O–S isotopic compositions of these intrusions.

The main Fe–Ti oxide ores represent accumulations of crystals that were directly derived from a normal basaltic magma within the Panzhihua magma chamber, rather than by the emplacement of Fe–Ti oxide-rich slurries or liquid immiscibility. The fO_2 of the Emeishan basaltic magmas estimated using the compositions of coexisting olivine and spinel from the Emeishan picrites reveals that the high-Ti series (FMQ + 1 ∼ FMQ + 2·5) are more oxidized than the low-Ti series (FMQ) in the Emeishan LIP. Thus, early saturation of Fe–Ti oxides was attributed to a moderately high oxygen fugacity instead of the enriched Fe–Ti content of the magma. The relatively oxidized nature of the parental magma is proposed to be inherited from an oxidized mantle source.

ACKNOWLEDGMENTS

We thank W.Q. Zheng and X. Li for the assistance with the WDS mapping and EMPA analyses, J. Hu for the ICP-MS analyses and Y.F. Yin for the PGE analyses. Helpful and constructive reviews by Steve Barnes, Steve Prevec and an anonymous reviewer were greatly appreciated and significantly improved the quality of this work. Additional and insightful comments and editorial handling by Jim Mungall also significantly contributed to improving the quality of this work.

FUNDING

This study was jointly supported by the Strategic Priority Research Program (B) of Chinese Academy of Sciences (XDB18000000) and the National Natural Science Foundation of China (41425011, 41873055 and 41473048).

SUPPLEMENTARY DATA

Supplementary data are available at *Journal of Petrology* online.

REFERENCES

Bai, Z. J., Zhong, H., Li, C., Zhu, W. G., He, D. F. & Qi, L. (2014). Contrasting parental magma compositions for The Hongge and Panzhihua Magmatic Fe–Ti-V oxide deposits, Emeishan Large Igneous Province, Sw China. *Economic Geology* **109**, 1763–1785.

Bai, Z. J., Zhong, H., Li, C., Zhu, W. G. & Hu, W. J. (2016). Association of cumulus apatite with compositionally unusual olivine and plagioclase in the Taihe Fe–Ti oxide ore-bearing layered mafic–ultramafic intrusion: petrogenetic significance and implications for ore genesis. *American Mineralogist* **101**, 2168–2175.

Bai, Z. J., Zhong, H., Li, C., Zhu, W. G. & Xu, G. W. (2012a). Platinum-group elements in the oxide layers of the Hongge mafic–ultramafic intrusion, Emeishan Large Igneous Province, SW China. *Ore Geology Reviews* **46**, 149–161.

Bai, Z. J., Zhong, H., Naldrett, A. J., Zhu, W. G. & Xu, G. W. (2012b). Whole-rock and mineral composition constraints on the genesis of the giant Hongge Fe–Ti-V oxide deposit in the Emeishan Large Igneous Province, Southwest China. *Economic Geology* **107**, 507–524.

Bai, Z. J., Zhong, H., Zhu, W. G., Hu, W. J. & Chen, C. J. (2019). The genesis of the newly discovered giant Wuben magmatic Fe–Ti oxide deposit in the Emeishan Large Igneous Province: a product of the late-stage redistribution and sorting of crystal slurries. *Mineralium Deposita* **54**, 31–46.

Ballhaus, C., Berry, R. F. & Green, D. H. (1990). Oxygen fugacity controls in the Earth's upper mantle. *Nature* **348**, 437–440.

Ballhaus, C., Berry, R. F. & Green, D. H. (1991). High pressure experimental calibration of the olivine-orthopyroxene-spinel oxygen geobarometer: implications for the oxidation state of the upper mantle. *Contributions to Mineralogy and Petrology* **107**, 27–40.

Barnes, S.-J. & Maier, W. D. (1999). The fractionation of Ni, Cu and the noble metals in silicate and sulphide Liquids. In: Keays, R. R., Lesher, C. M., Lightfoot, P. C. and Farrow, C. E. G. (eds) *Dynamic Processes in Magmatic Ore Deposits and Their Application to Mineral Exploration. Geological Association of Canada, Short Course Notes* **13**, 69–106.

Barnes, S.-J., Maier, W. D. & Curl, E. A. (2010). Composition of the marginal rocks and sills of the Rustenburg Layered Suite, Bushveld Complex, South Africa: implications for the formation of the platinum-group element deposits. *Economic Geology* **105**, 1491–1511.

Barnes, S. -J., Mungall, J. E. & Maier, W. D. (2015). Platinum group elements in mantle melts and mantle samples. *Lithos* **232**, 395–417.

Bowles, J. F. W., Prichard, H. M., Suarez, S. & Fisher, P. C. (2013). The first report of platinum-group minerals in magnetite-bearing gabbro, Freetown Layered Complex, Sierra Leone: occurrences and genesis. *Canadian Mineralogist* **51**, 455–473.

Buddington, A. F. & Lindsley, D. H. (1964). Iron-titanium oxide minerals and synthetic equivalents. *Journal of Petrology* **5**, 310–357.

Brenan, J. M., Finnigan, C. F., McDonough, W. F. & Homolova, V. (2012). Experimental constraints on the partitioning of Ru, Rh, Ir, Pt and Pd between chromite and silicate melt: the importance of ferric iron. *Chemical Geology* **302–303**, 16–32.

Brounce, M., Stolper, E. & Eiler, J. (2017). Redox variations in Mauna Kea lavas, the oxygen fugacity of the Hawaiian plume and the role of volcanic gases in Earth's oxygenation. *Proceedings of the National Academy of Sciences* **114**, 8997–9002.

Cawthorn, R. G. & Davies, G. (1983). Experimental data at 3 kbars pressure on parental magma to the Bushveld Complex. *Contributions to Mineralogy and Petrology* **83**, 128–135.

Cawthorn, R. G., Davies, G., Clubley-Armstrong, A. & McCarthy, T. S. (1981). Sills associated with the Bushveld Complex, South Africa: an estimate of the parental magma composition. *Lithos* **14**, 1–16.

Chai, G. & Naldrett, A. J. (1992). The Jinchuan Ultramafic intrusion: cumulate of a High-Mg basaltic magma. *Journal of Petrology* **33**, 277–303.

Charlier, B. & Grove, T. (2012). Experiments on liquid immiscibility along tholeiitic liquid lines of descent. *Contributions to Mineralogy and Petrology* **164**, 27–44.

Charlier, B., Namur, O., Bolle, O., Latypov, R. & Duchesne, J.-C. (2015). Fe–Ti–V–P ore deposits associated with Proterozoic massif-type anorthosites and related rocks. *Earth-Science Reviews* **141**, 56–81.

Charlier, B., Namur, O. & Grove, T. L. (2013). Compositional and kinetic controls on liquid immiscibility in ferrobasalt–rhyolite volcanic and plutonic series. *Geochimica et Cosmochimica Acta* **113**, 79–93.

Chen, J. F. & Jahn, B. M. (1998). Crustal evolution of southeastern China: Nd and Sr isotopic evidence. *Tectonophysics* **284**, 101–133.

Chen, L. M., Song, X. Y., Hu, R. Z., Yu, S. Y., He, H. L., Dai, Z. H., She, Y. W. & Xie, W. (2017). Controls on trace-element partitioning among co-crystallizing minerals: evidence from the Panzhihua layered intrusion, SW China. *American Mineralogist* **102**, 1006–1020.

Chen, Y., Xu, Y. G., Xu, T., Si, S. K., Liang, X. F., Tian, X. B., Deng, Y. F., Chen, L., Wang, P., Xu, Y. H., Lan, H. Q., Xiao, F. H., Li, W., Zhang, X., Yuan, X. H., Badal, J. & Teng, J. W. (2015). Magmatic underplating and crustal growth in the Emeishan Large Igneous Province, SW China, revealed by a passive seismic experiment. *Earth and Planetary Science Letters* **432**, 103–114.

Cherniak, D. J. & Liang, Y. (2012). Ti diffusion in natural pyroxene. *Geochimica et Cosmochimica Acta* **98**, 31–47.

Chiaradia, M. (2014). Copper enrichment in arc magmas controlled by overriding plate thickness. *Nature Geoscience* **7**, 43–46.

Chung, S.-L. & Jahn, B-M. (1995). Plume-lithosphere interaction in generation of the Emeishan flood basalts at the Permian-Triassic boundary. *Geology* **23**, 889–892.

Eales, H. V. (2000). Implications of the chromium budget of the Western Limb of the Bushveld Complex. *South African Journal of Geology* **103**, 141–150.

Eales, H. V. & Costin, G. (2012). Crustally contaminated Komatiite: primary source of the chromitites and marginal, lower and critical zone magmas in a staging chamber beneath the Bushveld Complex. *Economic Geology* **107**, 645–665.

Eiler, J. M. (2001). Oxygen isotope variations of basaltic lavas and upper mantle rocks. *Reviews in Mineralogy and Geochemistry* **43**, 319–364.

Ganino, C., Arndt, N., Zhou, M.-F., Gaillard, F. & Chauvel, C. (2008). Interaction of magma with sedimentary wall rock and magnetite ore genesis in the Panzhihua mafic intrusion, SW China. *Mineralium Deposita* **43**, 677–694.

Ganino, C., Harris, C., Arndt, N. T., Prevec, S. A. & Howarth, G. H. (2013). Assimilation of carbonate country rock by the parent magma of the Panzhihua Fe–Ti-V deposit (SW China): evidence from stable isotopes. *Geoscience Frontiers* **4**, 547–554.

Gao, S., Ling, W., Qiu, Y., Lian, Z., Hartmann, G. & Simon, K. (1999). Contrasting geochemical and Sm-Nd isotopic compositions of Archean metasediments from the Kongling high-grade terrain of the Yangtze craton: evidence for cratonic evolution and redistribution of REE during crustal anatexis. *Geochimica et Cosmochimica Acta* **63**, 2071–2088.

Gao, S., Luo, T. C., Zhang, B. R., Zhang, H. F., Han, Y. W., Zhao, Z. D. & Hu, Y. K. (1998). Chemical composition of the continental crust as revealed by studies in East China. *Geochimica et Cosmochimica Acta* **62**, 1959–1975.

Ghiorso, M. S. & Sack, R. O. (1995). Chemical mass transfer in magmatic processes IV. A revised and internally consistent thermodynamic model for the interpolation and extrapolation of liquid-solid equilibria in magmatic systems at elevated temperatures and pressures. *Contributions to Mineralogy and Petrology* **119**, 197–212.

Gibb, F. G. F. & Henderson, C. M. B. (2006). Chemistry of the Shiant Isles Main Sill, NW Scotland and wider implications for the petrogenesis of mafic sills. *Journal of Petrology* **47**, 191–230.

Gorring, M. L. & Naslund, H. R. (1995). Geochemical reversals within the lower 100 m of the Palisades sill, New Jersey. *Contributions to Mineralogy and Petrology* **119**, 263–276.

Gualda, G. A. R., Ghiorso, M. S., Lemons, R. V. & Carley, T. L. (2012). Rhyolite-MELTS: a modified calibration of MELTS optimized for silica-rich, fluid-bearing magmatic systems. *Journal of Petrology* **53**, 875–890.

Haddad, J. & Naslund, H. (2017). *Internal Stratigraphy of the Palisades Sill Olivine Zone: An Olivine Slurry Emplaced in a Hot Sill.* American Geophysical Union, Fall Meeting 2017, abstract #V23B-0484.

Hanski, E., Kamenetsky, V. S., Luo, Z.-Y., Xu, Y.-G. & Kuzmin, D. V. (2010). Primitive magmas in the Emeishan Large Igneous Province, southwestern China and northern Vietnam. *Lithos* **119**, 75–90.

Hart, S. R. & Dunn, T. (1993). Experimental cpx/melt partitioning of 24 trace elements. *Contributions to Mineralogy and Petrology* **113**, 1–8.

Hartley, M. E., Shorttle, O., Maclennan, J., Moussallam, Y. & Edmonds, M. (2017). Olivine-hosted melt inclusions as an archive of redox heterogeneity in magmatic systems. *Earth and Planetary Science Letters* **479**, 192–205.

Hayes, B., Bédard, J. H. & Lissenberg, C. J. (2015a). Olivine Slurry replenishment and the development of igneous layering in a Franklin Sill, Victoria Island, Arctic Canada. *Journal of Petrology* **56**, 83–112.

Hayes, B., Lissenberg, C. J., Bédard, J. H. & Beard, C. (2015b). The geochemical effects of olivine slurry replenishment and dolostone assimilation in the plumbing system of the Franklin Large Igneous Province, Victoria Island, Arctic Canada. *Contributions to Mineralogy and Petrology* **169**, 22.

Hill, E., Wood, B. J. & Blundy, J. D. (2000). The effect of Ca-Tschermaks component on trace element partitioning between clinopyroxene and silicate melt. *Lithos* **53**, 203–215.

Hill, R. & Roeder, P. (1974). The crystallization of spinel from basaltic liquid as a function of oxygen fugacity. *Journal of Geology* **82**, 709–729.

Holness, M. B., Farr, R. & Neufeld, J. A. (2017). Crystal settling and convection in the Shiant Isles Main Sill. *Contributions to Mineralogy and Petrology* **172**, 7.

Hoover, J. D. (1989). The chilled marginal gabbro and other contact rocks of the skaergaard intrusion. *Journal of Petrology* **30**, 441–476.

Hou, T., Zhang, Z. C., Encarnacion, J., Santosh, M. & Sun, Y. L. (2013). The role of recycled oceanic crust in magmatism and metallogeny: Os–Sr–Nd isotopes, U–Pb geochronology and geochemistry of picritic Dykes in the Panzhihua giant Fe–Ti oxide deposit, central Emeishan large igneous province, SW China. *Contributions to Mineralogy and Petrology* **165**, 805–822.

Hou, T., Zhang, Z. C. & Pirajno, F. (2012). A new metallogenic model of the Panzhihua giant V–Ti–iron oxide deposit (Emeishan Large Igneous Province) based on high-Mg olivine-bearing wehrlite and new field evidence. *International Geology Review* **54**, 1721–1745.

Howarth, G. H. & Prevec, S. A. (2013). Trace element, PGE and Sr–Nd isotope geochemistry of the Panzhihua mafic layered intrusion, SW China: Constraints on ore-forming processes and evolution of parent magma at depth in a plumbing-system. *Geochimica et Cosmochimica Acta* **120**, 459–478.

Howarth, G. H., Prevec, S. A. & Zhou, M.-F. (2013). Timing of Ti-magnetite crystallisation and silicate disequilibrium in the Panzhihua mafic layered intrusion: Implications for ore-forming processes. *Lithos* **170–171**, 73–89.

Jenkins, M. C. & Mungall, J. E. (2018). Genesis of the Peridotite Zone, Stillwater Complex, Montana, USA. *Journal of Petrology* **59**, 2157–2189.

Jenner, F. E. (2017). Cumulate causes for the low contents of sulfide-loving elements in the continental crust. *Nature Geoscience* **10**, 524–529.

Jugo, P. J. (2009). Sulfur content at sulfide saturation in oxidized magmas. *Geology* **37**, 415–418.

Jugo, P. J., Wilke, M. & Botcharnikov, R. E. (2010). Sulfur K-edge XANES analysis of natural and synthetic basaltic glasses: implications for S speciation and S content as function of oxygen fugacity. *Geochimica et Cosmochimica Acta* **74**, 5926–5938.

Kamenetsky, V. S., Chung, S.-L., Kamenetsky, M. B. & Kuzmin, D. V. (2012). Picrites from the Emeishan Large Igneous Province, SW China: a compositional continuum in primitive magmas and their respective mantle sources. *Journal of Petrology* **53**, 2095–2113.

Karykowski, B. T., Polito, P. A., Maier, W. D., Gutzmer, J. & Krause, J. (2017). New insights into the petrogenesis of the Jameson Range layered intrusion and associated

Fe-Ti-P-V-PGE-Au mineralisation, West Musgrave Province, Western Australia. *Mineralium Deposita* **52**, 233–255.

Keays, R. R. (1995). The role of komatiitic and picritic magmatism and S-saturation in the formation of ore deposits. *Lithos* **34**, 1–18.

Lee, C.-T. A., Luffi, P., Chin, E. J., Bouchet, R., Dasgupta, R., Morton, D. M., Le Roux, V., Yin, Q-Z. & Jin, D. (2012). Copper systematics in arc magmas and implications for crust-mantle differentiation. *Science* **336**, 64–68.

Li, C. & Ripley, E. M. (2009). Sulfur contents at sulfide-liquid or anhydrite saturation in silicate melts: empirical equations and example applications. *Economic Geology* **104**, 405–412.

Li, C., Tao, Y., Qi, L. & Ripley, E. M. (2012). Controls on PGE fractionation in the Emeishan picrites and basalts: constraints from integrated lithophile–siderophile elements and Sr–Nd isotopes. *Geochimica et Cosmochimica Acta* **90**, 12–32.

Liu, P. P., Zhou, M. F., Chen, W. T., Boone, M. & Cnudde, V. (2014a). Using multiphase solid inclusions to constrain the origin of the Baima Fe–Ti–(V) oxide deposit, SW China. *Journal of Petrology* **55**, 951–976.

Liu, P. P., Zhou, M. F., Wang, C. Y., Xing, C. M. & Gao, J. F. (2014b). Open magma chamber processes in the formation of the Permian Baima mafic–ultramafic layered intrusion, SW China. *Lithos* **184–187**, 194–208.

Luan, Y., Song, X. Y., Chen, L. M., Zheng, W. Q., Zhang, X. Q., Yu, S. Y., She, Y. W., Tian, X. L. & Ran, Q. Y. (2014). Key factors controlling the accumulation of the Fe–Ti oxides in the Hongge layered intrusion in the Emeishan Large Igneous Province, SW China. *Ore Geology Reviews* **57**, 518–538.

Ma, C. Q., Ehlers, C., Xu, C. H., Li, Z. C. & Yang, K. G. (2000). The roots of the Dabieshan ultrahigh-pressure metamorphic terrane: constraints from geochemistry and Nd–Sr isotope systematics. *Precambrian Research* **102**, 279–301.

Ma, Y., Ji, X. T., Li, J. C., Huang, M. & Kan, Z. Z. (2003). *Mineral Resources of the Panzhihua Region*. Chengdu: Sichuan Science and Technology Press.

Maier, W. D., Barnes, S.-J., Gartz, V. & Andrews, G. (2003). Pt-Pd reefs in magnetitites of the Stella layered intrusion, South Africa: a world of new exploration opportunities for platinum group elements. *Geology* **31**, 885–888.

Maier, W. D., Barnes, S.-J. & Karykowski, B. T. (2016). A chilled margin of komatiite and Mg-rich basaltic andesite in the western Bushveld Complex, South Africa. *Contributions to Mineralogy and Petrology* **171**, 1–22.

Matzen, A. K., Baker, M. B., Beckett, J. R. & Stolper, E. M. (2011). Fe–Mg partitioning between olivine and high-magnesian melts and the nature of Hawaiian parental liquids. *Journal of Petrology* **52**, 1243–1263.

McDonough, W. & Sun, S. (1995). The composition of the Earth. *Chemical Geology* **120**, 223–253.

Mondal, S. K. & Mathez, E. A. (2007). Origin of the UG2 chromitite layer, Bushveld Complex. *Journal of Petrology* **48**, 495–510.

Moussallam, Y., Edmonds, M., Scaillet, B., Peters, N., Gennaro, E., Sides, I. & Oppenheimer, C. (2016). The impact of degassing on the oxidation state of basaltic magmas: a case study of Kīlauea volcano. *Earth and Planetary Science Letters* **450**, 317–325.

Mungall, J. E., Hanley, J. J., Arndt, N. T. & Debecdelievre, A. (2006). Evidence from meimechites and other low-degree mantle melts for redox controls on mantle-crust fractionation of platinum-group elements. *Proceedings of the National Academy of Sciences* **103**, 12695–12700.

Mungall, J. E., Kamo, S. L. & McQuade, S. (2016). U–Pb geochronology documents out-of-sequence emplacement of ultramafic layers in the Bushveld Igneous Complex of South Africa. *Nature Communications* **7**, 13385.

Munteanu, M., Wilson, A. H., Costin, G., Yao, Y., Lum, J. E., Jiang, S.-Y., Jourdan, F., Chunnett, G. & Cioacă, M.-E. (2017). The Mafic–Ultramafic Dykes in the Yanbian Terrane (Sichuan Province, SW China): record of magma differentiation and emplacement in the Emeishan Large Igneous Province. *Journal of Petrology* **58**, 513–538.

Naldrett, A. J. (2010). Secular variation of magmatic sulfide deposits and their source magmas. *Economic Geology* **105**, 669–688.

Nielsen, T. F. D., Andersen, J. C. Ø., Holness, M. B., Keiding, J. K., Rudashevsky, N. S., Rudashevsky, V. N., Salmonsen, L. P., Tegner, C. & Veksler, I. V. (2015). The Skaergaard PGE and Gold Deposit: the result of in situ fractionation, sulphide saturation and magma chamber-scale precious metal redistribution by immiscible Fe-rich melt. *Journal of Petrology* **56**, 1643–1676.

Nielsen, R. L., Forsythe, L. M., Gallahan, W. E. & Fisk, M. R. (1994). Major- and trace-element magnetite-melt equilibria. *Chemical Geology* **117**, 167–191.

Owen-Smith, T. M. & Ashwal, L. D. (2015). Evidence for multiple pulses of crystal-bearing magma during emplacement of the Doros layered intrusion, Namibia. *Lithos* **238**, 120–139.

Pang, K.-N. (2008). *Origin of the Permian Panzhihua layered gabbroic intrusion and the hosted Fe-Ti-V oxide deposits, Sichuan Province, SW China*. Ph.D. thesis. University of Hong Kong, Hong Kong, 303 pp.

Pang, K.-N., Li, C., Zhou, M.-F. & Ripley, E. (2008a). Abundant Fe–Ti oxide inclusions in olivine from the Panzhihua and Hongge layered intrusions, SW China: evidence for early saturation of Fe–Ti oxides in ferrobasaltic magma. *Contributions to Mineralogy and Petrology* **156**, 307–321.

Pang, K.-N., Li, C., Zhou, M.-F. & Ripley, E. M. (2009). Mineral compositional constraints on petrogenesis and oxide ore genesis of the late Permian Panzhihua layered gabbroic intrusion, SW China. *Lithos* **110**, 199–214.

Pang, K.-N., Zhou, M.-F., Lindsley, D., Zhao, D. G. & Malpas, J. (2008b). Origin of Fe–Ti oxide Ores in Mafic intrusions: evidence from the Panzhihua Intrusion, SW China. *Journal of Petrology* **49**, 295–313.

Philpotts, A. R. & Doyle, C. D. (1983). Effect of magma oxidation state on the extent of silicate liquid immiscibility in a tholeiitic basalt. *American Journal of Science* **283**, 967–986.

Prendergast, M. D. (2000). Layering and Precious metals mineralization in the; Rincon del Tigre Complex, Eastern Bolivia. *Economic Geology* **95**, 113–130.

Prichard, H. M., Mondal, S. K., Mukherjee, R., Fisher, P. C. & Giles, N. (2017). Geochemistry and mineralogy of Pd in the magnetitite layer within the upper gabbro of the Mesoarchean Nuasahi Massif (Orissa, India). Mineralium Deposita **53**, 547–564.

Qi, L., Gao, J. F., Huang, X. W., Hu, J., Zhou, M.-F. & Zhong, H. (2011). An improved digestion technique for determination of platinum group elements in geological samples. *Journal of Analytical Atomic Spectrometry* **26**, 1900–1904.

Qi, L., Wang, C. Y. & Zhou, M.-F. (2008). Controls on the PGE distribution of Permian Emeishan alkaline and peralkaline volcanic rocks in Longzhoushan, Sichuan Province, SW China. *Lithos* **106**, 222–236.

Qi, L. & Zhou, M. (2008). Platinum-group elemental and Sr–Nd–Os isotopic geochemistry of Permian Emeishan flood basalts in Guizhou Province, SW China. *Chemical Geology* **248**, 83–103.

Qi, L., Zhou, M. F. & Wang, C. Y. (2004). Determination of low concentrations of platinum group elements in geological samples by ID-ICP-MS. *Journal of Analytical Atomic Spectrometry* **19**, 1335–1339.

Raedeke, L. D. (1979). Stratigraphy and petrology of the Stillwater Complex, Montana. Unpublished M.Sc. thesis, University of Washington Seattle, 109pp.

Ren, Z. Y., Wu, Y. D., Zhang, L., Nichols, A. R. L., Hong, L. B., Zhang, Y. H., Zhang, Y., Liu, J. Q. & Xu, Y. G. (2017). Primary magmas and mantle sources of Emeishan basalts constrained from major element, trace element and Pb isotope compositions of olivine-hosted melt inclusions. *Geochimica et Cosmochimica Acta* **208**, 63–85.

Roeder, P. L. & Campbell, I. H. (1985). The effect of postcumulus reactions on composition of chrome-spinels from the Jimberlana Intrusion. *Journal of Petrology* **26**, 763–786.

Sa, J. H. S., Barnes, S.-J., Prichard, H. M. & Fisher, P. C. (2005). The distribution of base metals and platinum-group elements in magnetitite and its host rocks in the Rio Jacare Intrusion, Northeastern Brazil. *Economic Geology* **100**, 333–348.

Sharpe, M. R. (1981). The chronology of magma influxes to the eastern compartment of the Bushveld Complex as exemplified by its marginal border groups. *Journal of the Geological Society* **138**, 307–326.

Sharpe, M. R. & Hulbert, L. J. (1985). Ultramafic sills beneath the eastern Bushveld Complex; mobilized suspensions of early lower zone cumulates in a parental magma with boninitic affinities. *Economic Geology* **80**, 849–871.

She, Y. W., Song, X. Y., Chen, L. M., Yu, S. Y., Zhu, X. K., Yi, J. N. & Hu, J. H. (2017). Platinum-group element geochemistry of the layered intrusions in the Emeishan large igneous province, SW China: Implications for the principal controls on magmatic sulfide immiscibility. *American Journal of Science* **317**, 483–513.

She, Y. W., Yu, S. Y., Song, X. Y., Chen, L. M., Zheng, W. Q. & Luan, Y. (2014). The formation of P-rich Fe–Ti oxide ore layers in the Taihe layered intrusion, SW China: implications for magma-plumbing system process. *Ore Geology Reviews* **57**, 539–559.

Shellnutt, J. G., Denyszyn, S. W. & Mundil, R. (2012). Precise age determination of mafic and felsic intrusive rocks from the Permian Emeishan large igneous province (SW China). *Gondwana Research* **22**, 118–126.

Shellnutt, J. G., Ma, G. S. K. & Qi, L. (2015). Platinum-group elemental chemistry of the Baima and Taihe Fe–Ti oxide bearing gabbroic intrusions of the Emeishan large igneous province, SW China. *Chemie der Erde - Geochemistry* **75**, 35–49.

Shellnutt, J. G. & Zhou, M.-F. (2007). Permian peralkaline, peraluminous and metaluminous A-type granites in the Panxi district, SW China: their relationship to the Emeishan mantle plume. *Chemical Geology* **243**, 286–316.

Sisson, T. W. (2003). Native gold in a Hawaiian alkalic magma. *Economic Geology* **98**, 643–648.

Song, X. Y., Keays, R. R., Xiao, L., Qi, H. W. & Ihlenfeld, C. (2009). Platinum-group element geochemistry of the continental flood basalts in the central Emeisihan Large Igneous Province, SW China. *Chemical Geology* **262**, 246–261.

Song, X. Y., Qi, H. W., Hu, R. Z., Chen, L. M., Yu, S. Y. & Zhang, J. F. (2013). Formation of thick stratiform Fe–Ti oxide layers in layered intrusion and frequent replenishment of fractionated mafic magma: evidence from the Panzhihua intrusion, SW China. *Geochemistry, Geophysics, Geosystems* **14**, 712–732.

Song, X. Y., Zhou, M. F., Cao, Z. M., Sun, M. & Wang, Y. L. (2003). Ni–Cu–(PGE) magmatic sulfide deposits in the Yangliuping area, Permian Emeishan igneous province, SW China. *Mineralium Deposita* **38**, 831–843.

Song, X. Y., Zhou, M. F., Tao, Y. & Xiao, J. F. (2008). Controls on the metal compositions of magmatic sulfide deposits in the Emeishan large igneous province, SW China. *Chemical Geology* **253**, 38–49.

Sorensen, H. S. & Wilson, J. R. (1995). A strontium and neodymium isotopic investigation of the Fongen–Hyllingen Layered Intrusion, Norway. *Journal of Petrology* **36**, 161–187.

Tang, Q., Li, C., Tao, Y., Ripley, E. M. & Xiong, F. (2017). Association of Mg-rich Olivine with magnetite as a result of brucite marble assimilation by Basaltic Magma in the Emeishan Large Igneous Province, SW China. *Journal of Petrology* **58**, 699–714.

Tang, Q. Y., Ma, Y. S., Zhang, M. J., Li, C., Zhu, D. & Tao, Y. (2013). The Origin of Ni–Cu-PGE sulfide mineralization in the margin of the Zhubu Mafic–ultramafic Intrusion in the Emeishan Large Igneous Province, Southwestern China. *Economic Geology* **108**, 1889–1901.

Tao, Y., Li, C., Hu, R. Z., Ripley, E. M., Du, A. D. & Zhong, H. (2007). Petrogenesis of the Pt–Pd mineralized Jinbaoshan ultramafic intrusion in the Permian Emeishan Large Igneous Province, SW China. *Contributions to Mineralogy and Petrology* **153**, 321–337.

Tao, Y., Li, C., Song, X. Y. & Ripley, E. M. (2008). Mineralogical, petrological and geochemical studies of the Limahe mafic–ultramatic intrusion and associated Ni–Cu sulfide ores, SW China. *Mineralium Deposita* **43**, 849–872.

Tao, Y., Putirka, K., Hu, R.-Z. & Li, C. (2015). The magma plumbing system of the Emeishan large igneous province and its role in basaltic magma differentiation in a continental setting. *American Mineralogist* **100**, 2509–2517.

Tegner, C., Wilson, J. R. & Brooks, C. K. (1993). Intraplutonic Quench Zones in the Kap Edvard Holm Layered Gabbro Complex, East Greenland. *Journal of Petrology* **34**, 681–710.

Toplis, M. J. & Carroll, M. R. (1995). An experimental study of the influence of oxygen fugacity on Fe–Ti oxide stability, phase relations and mineral–melt equilibria in ferro-basaltic systems. *Journal of Petrology* **36**, 1137–1170.

Voordouw, R., Gutzmer, J. & Beukes, N. (2009). Intrusive origin for Upper Group (UG1, UG2) stratiform chromitite seams in the Dwars River area, Bushveld Complex, South Africa. *Mineralogy and Petrology* **97**, 75–94.

Wager, L. R. (1960). The major element variation of the layered series of the Skaergaard intrusion and a re-estimation of the average composition of the hidden layered series and of the successive residual magmas. *Journal of Petrology* **1**, 364–398.

Wang, C. Y. & Zhou, M.-F. (2006). Genesis of the Permian Baimazhai magmatic Ni–Cu–(PGE) sulfide deposit, Yunnan, SW China. *Mineralium Deposita* **41**, 771–783.

Wang, C. Y., Zhou, M.-F. & Keays, R. (2006). Geochemical constraints on the origin of the Permian Baimazhai mafic–ultramafic intrusion, SW China. *Contributions to Mineralogy and Petrology* **152**, 309–321.

Wang, C. Y., Zhou, M.-F. & Qi, L. (2007). Permian flood basalts and mafic intrusions in the Jinping (SW China)-Song Da (northern Vietnam) district: Mantle sources, crustal contamination and sulfide segregation. *Chemical Geology* **243**, 317–343.

Wang, C. Y., Zhou, M.-F., Yang, S., Qi, L. & Sun, Y. (2014). Geochemistry of the Abulangdang intrusion: Cumulates of high-Ti picritic magmas in the Emeishan large igneous province, SW China. *Chemical Geology* **378–379**, 24–39.

Wang, C. Y., Zhou, M.-F. & Zhao, D. (2005). Mineral chemistry of chromite from the Permian Jinbaoshan Pt-Pd-sulphide-bearing ultramafic intrusion in SW China with petrogenetic implications. *Lithos* **83**, 47–66.

Wang, J., Wang, Q., Zhang, C., Dan, W., Qi, Y., Zhang, X.-Z. & Xia, X.-P. (2018). Late Permian Bimodal Volcanic Rocks in

the Northern Qiangtang Terrane, Central Tibet: evidence for interaction between the Emeishan Plume and the Paleo-Tethyan Subduction System. *Journal of Geophysical Research: Solid Earth* **123**, 6540–6561.

Wang, M., Zhang, Z. C., Santosh, M. & Hou, T. (2014). Geochemistry of Late Permian picritic porphyries and associated Pingchuan iron ores, Emeishan Large Igneous Province, Southwest China: constraints on petrogenesis and iron sources. *Ore Geology Reviews* **57**, 602–617.

Wilson, A. H. (2012). A chill sequence to the Bushveld Complex: insight into the first stage of emplacement and implications for the parental magmas. *Journal of Petrology* **53**, 1123–1168.

Wilson, A. H. (2015). The earliest stages of emplacement of the eastern Bushveld Complex: development of the lower zone, marginal zone and basal ultramafic sequence. *Journal of Petrology* **56**, 347–388.

Xiao, L., Xu, Y. G., Mei, H. J., Zheng, Y. F., He, B. & Pirajno, F. (2004). Distinct mantle sources of low-Ti and high-Ti basalts from the western Emeishan large igneous province, SW China: implications for plume-lithosphere interaction. *Earth and Planetary Science Letters* **228**, 525–546.

Xing, C. M., Wang, C. Y. & Li, C. (2014). Trace element compositions of apatite from the middle zone of the Panzhihua layered intrusion, SW China: Insights into the differentiation of a P- and Si-rich melt. *Lithos* **204**, 188–202.

Xu, Y. G. & Chung, S.-L. (2001). The Emeishan Large Igneous Province: evidence for mantle plume activity and melting conditions. *Geochemica* **20**, 1–9 (in chinese with english abstract).

Xu, Y. G., Chung, S. -L., Jahn, B. M. & Wu, G. Y. (2001). Petrologic and geochemical constraints on the petrogenesis of Permian-Triassic Emeishan flood basalts in southwestern China. *Lithos* **58**, 145–168.

Xu, Y. G. & He, B. (2007). Thick, high-velocity crust in the Emeishan large igneous province, southwestern China: Evidence for crustal growth by magmatic underplating or intraplating. *Geological Society of America Special Papers* **430**, 841–858.

Xu, J. F., Suzuki, K., Xu, Y. G., Mei, H. J. & Li, J. (2007). Os, Pb and Nd isotope geochemistry of the Permian Emeishan continental flood basalts: insights into the source of a large igneous province. *Geochimica et Cosmochimica Acta* **71**, 2104–2119.

Yao, Z. S., Qin, K. Z. & Mungall, J. E. (2018). Tectonic controls on Ni and Cu contents of primary mantle-derived magmas for the formation of magmatic sulfide deposits. *American Mineralogist* **103**, 1545–1567.

Yu, S.-Y., Shen, N.-P., Song, X.-Y., Ripley, E. M., Li, C. & Chen, L.-M. (2017). An integrated chemical and oxygen isotopic study of primitive olivine grains in picrites from the Emeishan Large Igneous Province, SW China: Evidence for oxygen isotope heterogeneity in mantle sources. *Geochimica et Cosmochimica Acta* **215**, 263–276.

Yu, S. Y., Song, X. Y., Ripley, E. M., Li, C., Chen, L. M., She, Y. W. & Luan, Y. (2015). Integrated O–Sr–Nd isotope constraints on the evolution of four important Fe–Ti oxide ore-bearing mafic–ultramafic intrusions in the Emeishan large igneous province, SW China. *Chemical Geology* **401**, 28–42.

Zhang, X. Q., Song, X. Y., Chen, L. M., Xie, W., Yu, S. Y., Zheng, W. Q., Deng, Y. F., Zhang, J. F. & Gui, S. G. (2012). Fractional crystallization and the formation of thick Fe–Ti–V oxide layers in the Baima layered intrusion, SW China. *Ore Geology Reviews* **49**, 96–108.

Zhang, X. Q., Song, X. Y., Chen, L. M., Yu, S. Y., Xie, W., Deng, Y., Zhang, J. F. & Gui, S. G. (2013). Chalcophile element geochemistry of the Baima layered intrusion, Emeishan Large Igneous Province, SW China: implications for sulfur saturation history and genetic relationship with high-Ti basalts. *Contributions to Mineralogy and Petrology* **166**, 193–209.

Zhang, Z. C., Mahoney, J. J., Mao, J. W. & Wang, F. S. (2006). Geochemistry of Picritic and Associated Basalt Flows of the Western Emeishan Flood Basalt Province, China. *Journal of Petrology* **47**, 1997–2019.

Zhang, Z. C., Mao, J. W., Saunders, A. D., Ai, Y., Li, Y. & Zhao, L. (2009). Petrogenetic modeling of three mafic–ultramafic layered intrusions in the Emeishan large igneous province, SW China, based on isotopic and bulk chemical constraints. *Lithos* **113**, 369–392.

Zhong, H., Campbell, I. H., Zhu, W. G., Allen, C. M., Hu, R. Z., Xie, L. W. & He, D. F. (2011a). Timing and source constraints on the relationship between mafic and felsic intrusions in the Emeishan large igneous province. *Geochimica et Cosmochimica Acta* **75**, 1374–1395.

Zhong, H., Hu, R. Z., Wilson, A. & Zhu, W. G. (2005). Review of the Link between the Hongge Layered Intrusion and Emeishan Flood Basalts, Southwest China. *International Geology Review* **47**, 971–985.

Zhong, H., Qi, L., Hu, R. Z., Zhou, M. F., Gou, T. Z., Zhu, W. G., Liu, B. G. & Chu, Z. Y. (2011b). Rhenium-osmium isotope and platinum-group elements in the Xinjie layered intrusion, SW China: implications for source mantle composition, mantle evolution, PGE fractionation and mineralization. *Geochimica et Cosmochimica Acta* **75**, 1621–1641.

Zhong, H., Yao, Y., Prevec, S. A., Wilson, A. H., Viljoen, M. J., Viljoen, R. P., Liu, B.-G. & Luo, Y.-N. (2004). Trace-element and Sr–Nd isotopic geochemistry of the PGE-bearing Xinjie layered intrusion in SW China. *Chemical Geology* **203**, 237–252.

Zhong, H., Zhu, W. G., Chu, Z. Y., He, D.-F. & Song, X. Y. (2007). Shrimp U-Pb zircon geochronology, geochemistry and Nd-Sr isotopic study of contrasting granites in the Emeishan large igneous province, SW China. *Chemical Geology* **236**, 112–133.

Zhou, M.-F., Arndt, N. T., Malpas, J., Wang, C. Y. & Kennedy, A. K. (2008). Two magma series and associated ore deposit types in the Permian Emeishan large igneous province, SW China. *Lithos* **103**, 352–368.

Zhou, M.-F., Chen, W. T., Wang, C. Y., Prevec, S. A., Liu, P. P. & Howarth, G. H. (2013). Two stages of immiscible liquid separation in the formation of Panzhihua-type Fe–Ti-V oxide deposits, SW China. *Geoscience Frontiers* **4**, 481–502.

Zhou, M.-F., Malpas, J., Song, X.-Y., Robinson, P. T., Sun, M., Kennedy, A. K., Lesher, C. M. & Keays, R. R. (2002). A temporal link between the Emeishan large igneous province (SW China) and the end-Guadalupian mass extinction. *Earth and Planetary Science Letters* **196**, 113–122.

Zhou, M.-F., Robinson, P. T., Lesher, C. M., Keays, R. R., Zhang, C.-J. & Malpas, J. (2005). Geochemistry, petrogenesis and metallogenesis of the Panzhihua Gabbroic Layered Intrusion and associated Fe–Ti-V oxide deposits, Sichuan Province, SW China. *Journal of Petrology* **46**, 2253–2280.